CHAPTER IV
RESULTS AND DISCUSSION

4.1 Standard Analysis Chromatogram

The standard substances, which are *tert*-butanol, cyclohexene (4.84 wt.% in *tert*-butanol), cyclohexene oxide (4.91 wt.% in *tert*-butanol), 2-cyclohexen-1-ol (5.06 wt.% in *tert*-butanol), 2-cyclohexen-1-one (5.48 wt.% in *tert*-butanol), and (1S,2S)-*tran*-1,2-cyclohexanediol (5.17 wt.% in *tert*-butanol) were mixed with dodecane (5.04 wt.% in *tert*-butanol), which is internal standard. The mixture was analyzed by a GC-FID following the conditions for product analysis, as described in Chapter III. The chromatogram of the mixture is shown in Figure 4.1.

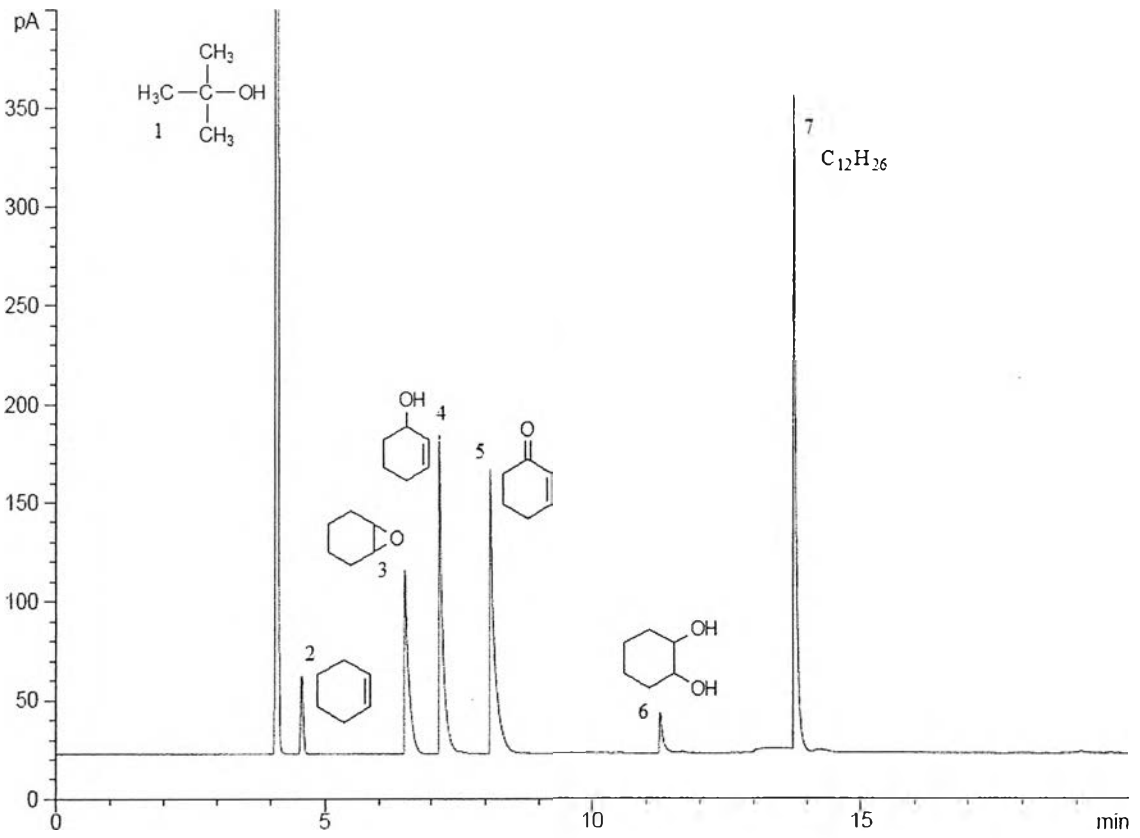

Figure 4.1 Chromatogram of the mixed standards: (1) *tert*-butanol, (2) cyclohexene, (3) cyclohexene oxide, (4) 2-cyclohexen-1-ol, (5) 2-cyclohexen-1-one, (6) (1S,2S)-*trans*-1,2-cyclohexanediol, and (7) dodecane.

The retention time and response factor of cyclohexene, cyclohexene oxide, 2-cyclohexen-1-ol, 2-cyclohexen-1-one, (1S,2S)-*trans*-1,2-cyclohexanediol, and dodecane are shown in Table 4.1.

Table 4.1 Retention time and response factor of each substance from GC analysis

Number	Substance	Retention time (min)	Response factor
1	*tert*-Butanol (solvent)	4.08	-
2	cyclohexene	4.57	0.38
3	cyclohexene oxide	6.66	0.47
4	2-cyclohexen-1-ol	7.42	0.59
5	2-cyclohexen-1-one	8.40	0.58
6	(1S,2S)-*trans*-1,2-cyclohexanediol	11.48	0.61
7	dodecane	14.00	1.00

Moreover, from the Table 4.1, the retention time of dodecane, which is internal standard, was detected at 14.0 min, obviously separating from the reactant and possible products. It could be pointed out that dodecane was suitable to be an internal standard for this reaction.

From Chapter III, the response factors of each product are calculated based on the following formula:

$$R_x = \left(\frac{m_{is}}{A_{is}}\right)\left(\frac{A_X}{m_x}\right)$$

4.2 Catalyst Characterizations

4.2.1 TG-DTA Analysis

The TG-DTA curves were used to determine thermal decomposition of the uncalcined TiO_2 (SG) and to obtain its suitable calcination temperature. Figure 4.2 shows the TG-DTA curves of the uncalcined TiO_2 (SG) (a) without RuO_2 loading, and (b) with 1 mol% RuO_2 loading by the SSSG method. The comparable total weight losses measured from the TG curve were 40.4 and 40.3 wt.% for uncalcined TiO_2 (SG) and RuO_2/TiO_2 (SSSG), respectively. The DTA curves show three main exothermic regions. The details of the position of the exothermic peaks, as well as their corresponding weight loss, are summarized in Table 4.2. The first small exothermic peak, with its position lower than 150°C, is due to the removal of loosely bound water from the surface of nanocrystals. The second exothermic peak between 150 and 350°C is very sharp and narrow and is attributed to the decomposition of the organic surfactant template (LAHC), and modifying agent (ACA). The third exothermic region between 350 and 500°C consists of two weaker peaks, which correspond to the crystallization of anatase TiO_2 structure and also the elimination of organic remnants and chemisorbed water (Sakulkhaemaruethai *et al.*, 2004). The distinct difference of the thermal decomposition behavior of the varied RuO_2/TiO_2 (SSSG) gel from the dried unloaded one is that there is difference of intensity of exothermic peaks in the DTA curves. However, there is insignificant weight loss observed from TG curves of uncalcined TiO_2 (SG) and RuO_2/TiO_2 (SSSG) gels beyond the calcination temperature of 500°C. Consequently, the results confirm that the calcination temperature of 500°C was adequate for complete surfactant removal, as well as the crystallization of anatase TiO_2 structure.

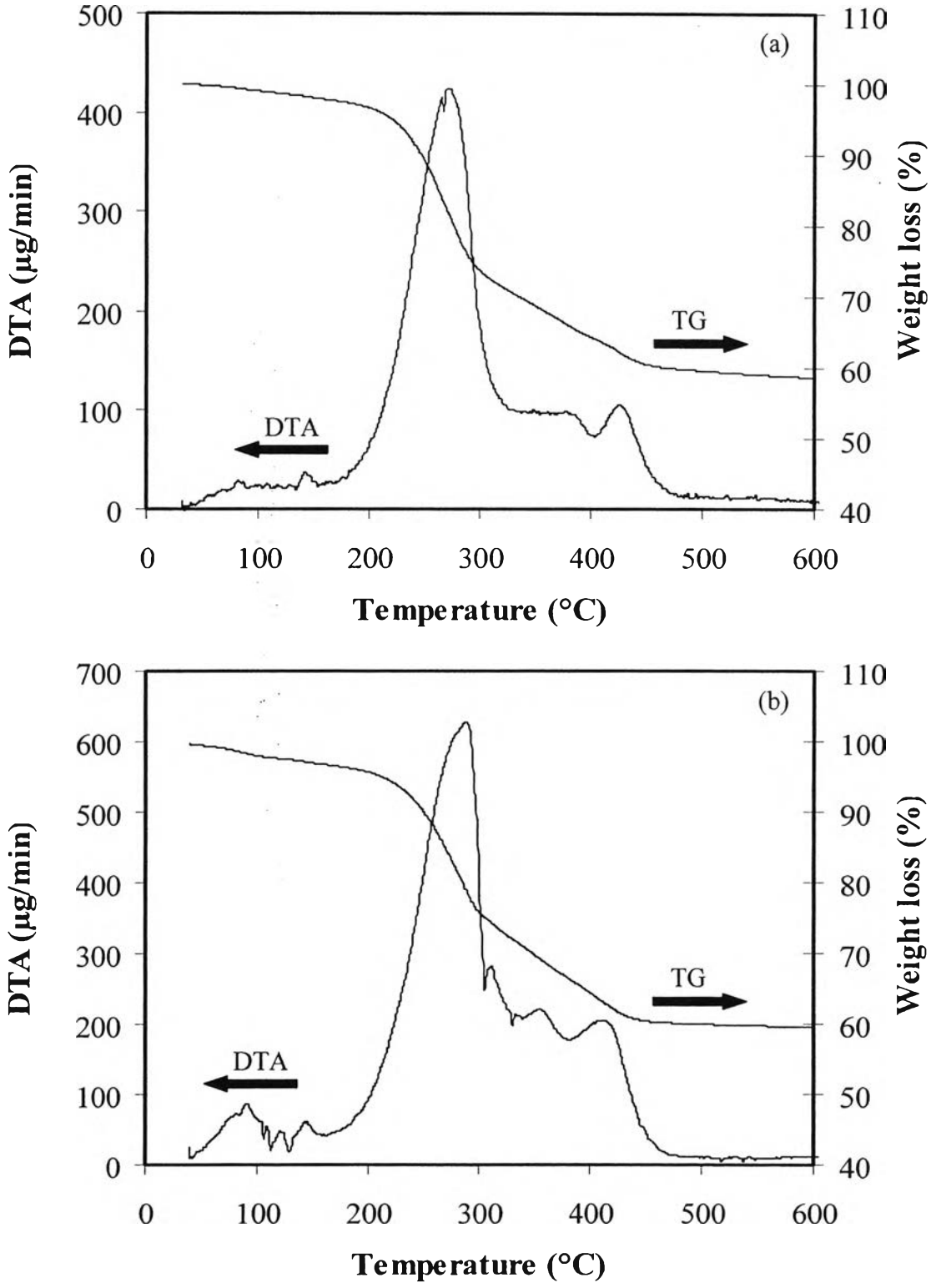

Figure 4.2 TG-DTA curves of (a) uncalcined TiO_2 (SG) and (b) uncalcined 1 mol% RuO_2/TiO_2 (SSSG).

Table 4.2 Thermal decomposition behavior of the uncalcined TiO_2 (SG) and uncalcined 1 mol% RuO_2/TiO_2 (SSSG) from TG-DTA analysis

Catalyst	Position of exothermic peak (°C)				Corresponding weight loss (wt.%)				
	1st peak	2nd peak	3rd peak	4th peak	1st peak	2nd peak	3rd peak	4th peak	Total
uncalcined TiO_2 (SG)	82.3	271.0	377.6	425.6	2.0	29.3	4.6	4.5	40.4
uncalcined 1 mol% RuO_2/TiO_2 (SSSG)	90.5	288.8	354.2	411.9	3.1	24.6	5.5	7.1	40.3

Moreover, TGA was also employed to determine of the surface OH density (OH/nm^2) and surface OH-to-catalyst weight ratio (OH/g). Figures 4.3–4.5 show TGA curves of RuO_2/TiO_2 (IWI) calcined at different temperatures, times, and with different RuO_2 loading, respectively. Figure 4.6 shows TGA curves RuO_2/TiO_2 (SSSG) with different RuO_2 loading. The TGA curves can be divided in two regions. The first region, with a temperature range from 100 to 120°C (or heating time from 3.5 to 4.5 min), was attributable to the removal of physically adsorbed water, where this region is not crucial for powder characterization as it depends even on humidity during sample preparation. The second region, with a temperature range from 120 to 500°C (or heating time from 4.5 to 23.5 min), represented the weight loss by the removal of hydroxyl groups from the powder surface and possibly desorption of volatile organic compounds associated with powder synthesis or processing. The details of the OH/nm^2 and OH/g are summarized in Tables 4.3 and 4.4.

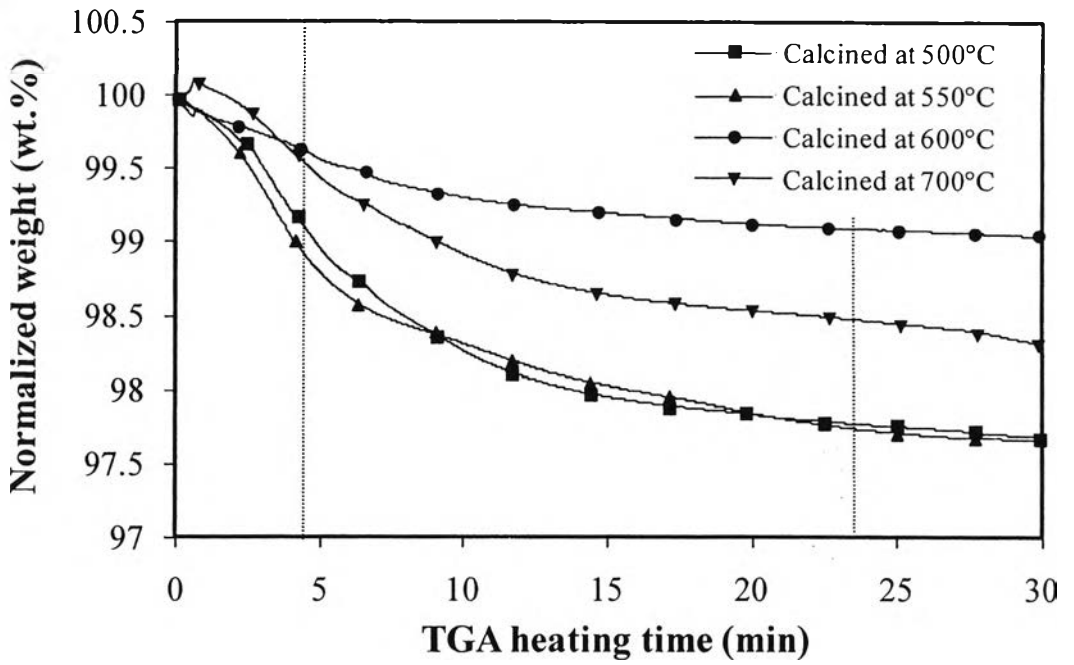

Figure 4.3 TGA comparison of 1 mol% RuO_2/TiO_2 (IWI) calcined for 4 h with different calcination temperatures. The surface OH is based on the weight loss of between 120 and 500°C.

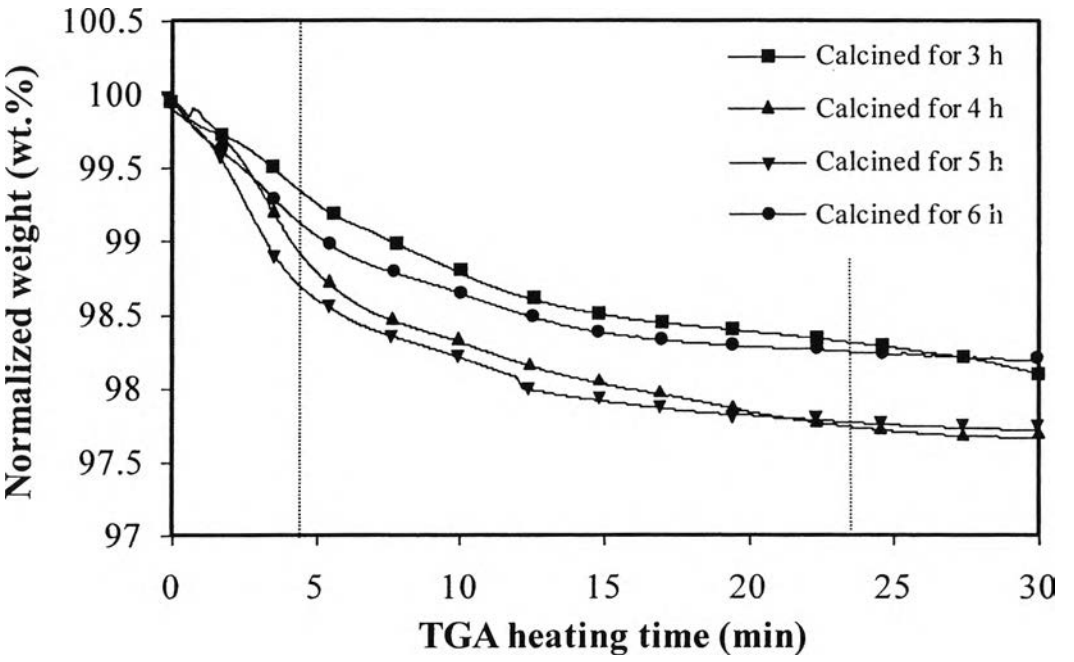

Figure 4.4 TGA comparison of 1 mol% RuO_2/TiO_2 (IWI) calcined at 550°C with different calcination times. The surface OH is based on the weight loss of between 120 and 500°C.

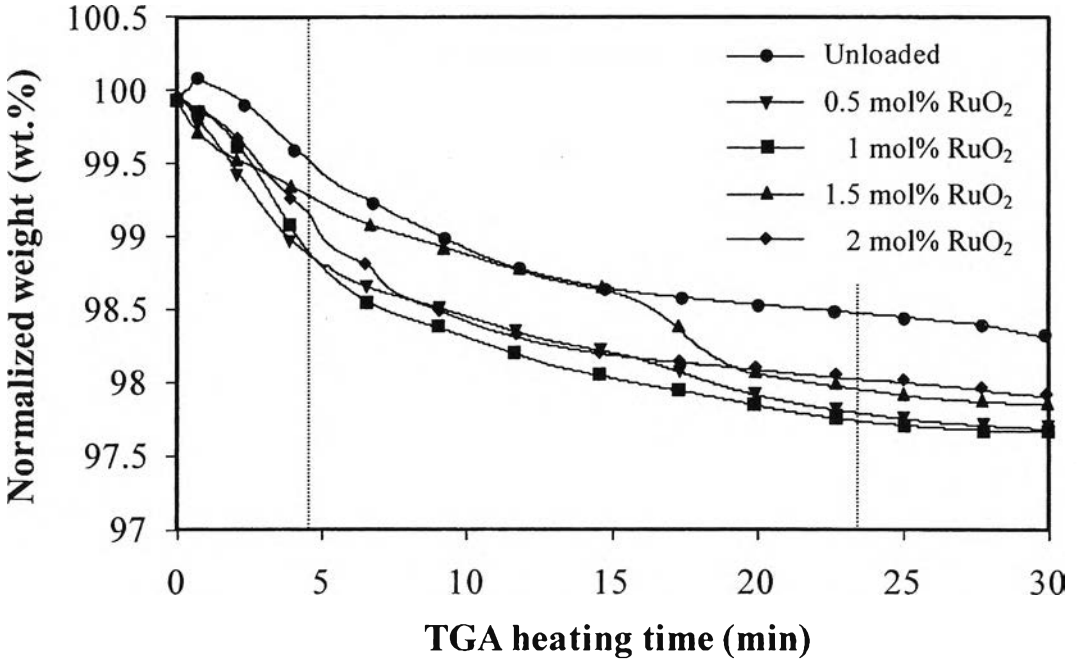

Figure 4.5 TGA comparison of RuO_2/TiO_2 (IWI) calcined at 550°C for 4 h with different RuO_2 loading. The OH surface is based on the weight loss of between 120 and 500°C.

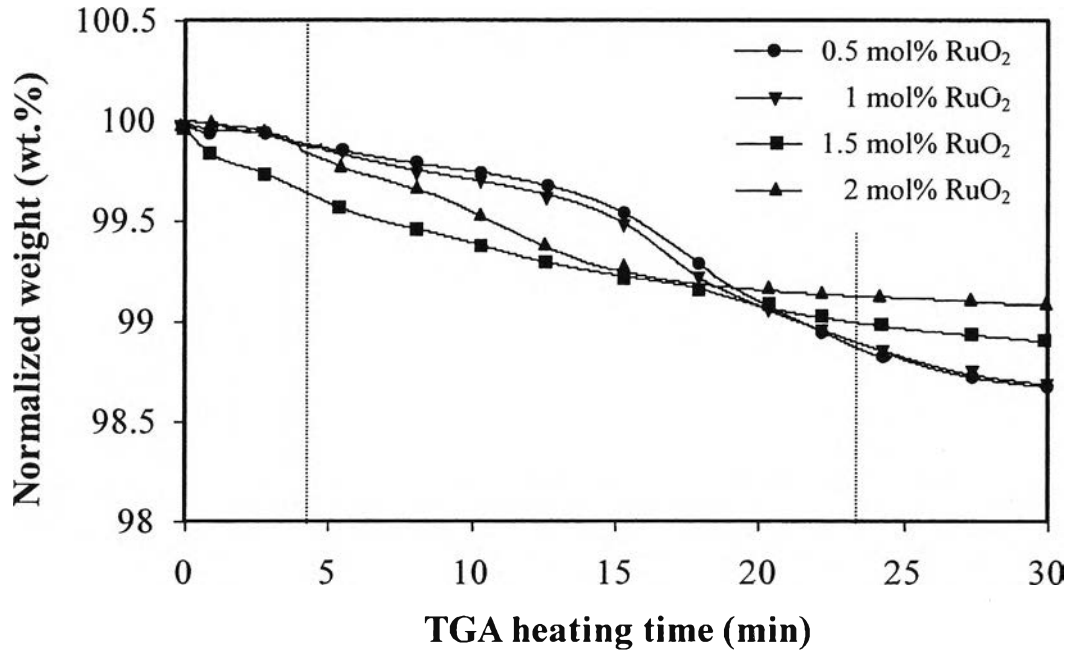

Figure 4.6 TGA comparison of RuO_2/TiO_2 (SSSG) calcined at 550°C for 4 h with different RuO_2 loading. The OH surface is based on the weight loss of between 120 and 500°C.

Table 4.3 Surface OH density (OH/nm^2) and surface OH-to-catalyst weight ratio (OH/g) of RuO_2/TiO_2 (IWI)

Catalyst	RuO_2 content (mol%)	Calcination temperature (°C)	Calcination time (h)	$w_{120°C}$ (mg)	$w_{500°C}$ (mg)	OH/nm^2	$OH/g(\times10^{-20})$
RuO_2/TiO_2 (IWI)	1	500	4	12.39	12.26	9.02	4.71
		550		18.17	18.01	10.04	3.92
		600		16.93	16.86	8.75	1.86
		700		21.84	21.83	7.58	0.21
	1	550	3	7.73	7.66	9.79	3.99
			5	12.70	12.60	11.43	3.13
			6	11.47	11.40	10.74	2.71
	0	550	4	14.29	14.14	11.05	4.65
	0.5			13.16	13.03	11.09	4.37
	1.5			14.03	13.92	9.45	3.51
	2			8.00	7.94	9.10	3.36

Table 4.4 Surface OH density (OH/nm^2) and surface OH-to-catalyst weight ratio (OH/g) of RuO_2/TiO_2 (SSSG)

Catalyst	RuO_2 content (mol%)	Calcination temperature (°C)	Calcination time (h)	$w_{120°C}$ (mg)	$w_{500°C}$ (mg)	OH/nm^2	$OH/g(\times10^{-20})$
RuO_2/TiO_2 (SSSG)	0.5	550	4	17.91	17.71	16.27	4.85
	1			21.94	21.70	18.19	4.73
	1.5			12.97	12.88	12.45	3.05
	2			16.67	16.56	12.48	2.90

The results from TGA analysis show the change of surface OH-to-catalyst weight ratio (OH/g) with respect to the calcination temperature, calcination time, and RuO_2 loading. It can be clearly seen that surface OH-to-catalyst weight ratio decreased with increasing calcination temperature, calcination time, and also RuO_2 loading.

4.2.2 N_2 Adsorption-Desorption Analysis

The N_2 adsorption-desorption measurement at liquid N_2 temperature of -196°C was used to examine mesoporosity and textural properties of the catalysts. The shape of the isotherms exhibits the characteristic behavior of the structure of powder, which is composed of an assembly of particles with large open packing. The N_2 adsorption-desorption isotherms of the TiO_2 (SG), 1 mol% RuO_2/TiO_2 (IWI), and 1 mol% RuO_2/TiO_2 (SSSG) calcined at 550°C for 4 h are shown in Figures 4.7 to 4.9, respectively. It can be seen that they exhibit typical IUPAC type IV pattern with hysteresis loop, which is characteristic of mesoporous-assembled structure (mesoporous size between 2 and 50 nm) according to the classification of IUPAC (Rouquerol *et al.*, 1999). A sharp increase in adsorption volume of N_2 was observed and located in the P/P_0 range of 0.45-0.85. This sharp increase can be attributed to the capillary condensation of N_2 inside the mesopores, indicating the good homogeneity of the sample and fairly small pore size since the P/P_0 position of the inflection point is directly related to the pore dimension. As illustrated in the inset of Figures 4.7 to 4.9, the pore size distribution curve was calculated from the desorption branch of the isotherms by the BJH method. The samples possess monomodal and very narrow pore size distribution, identifying good quality of the samples.

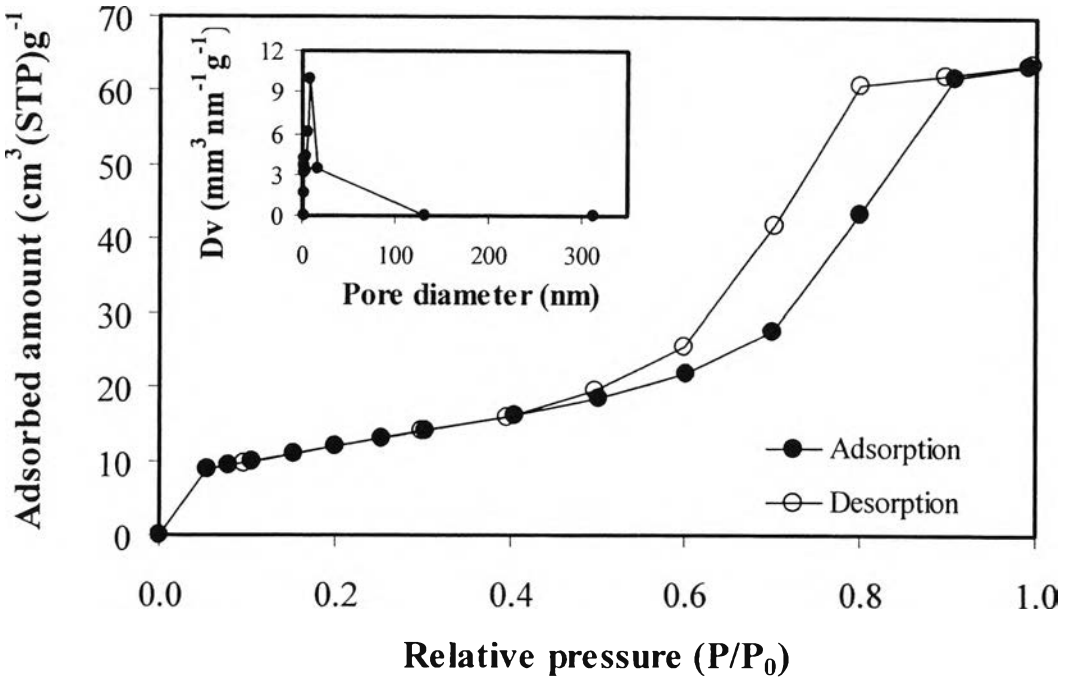

Figure 4.7 N_2 adsorption-desorption isotherms of the TiO_2 (SG) calcined at 550°C for 4 h (Inset: pore size distribution).

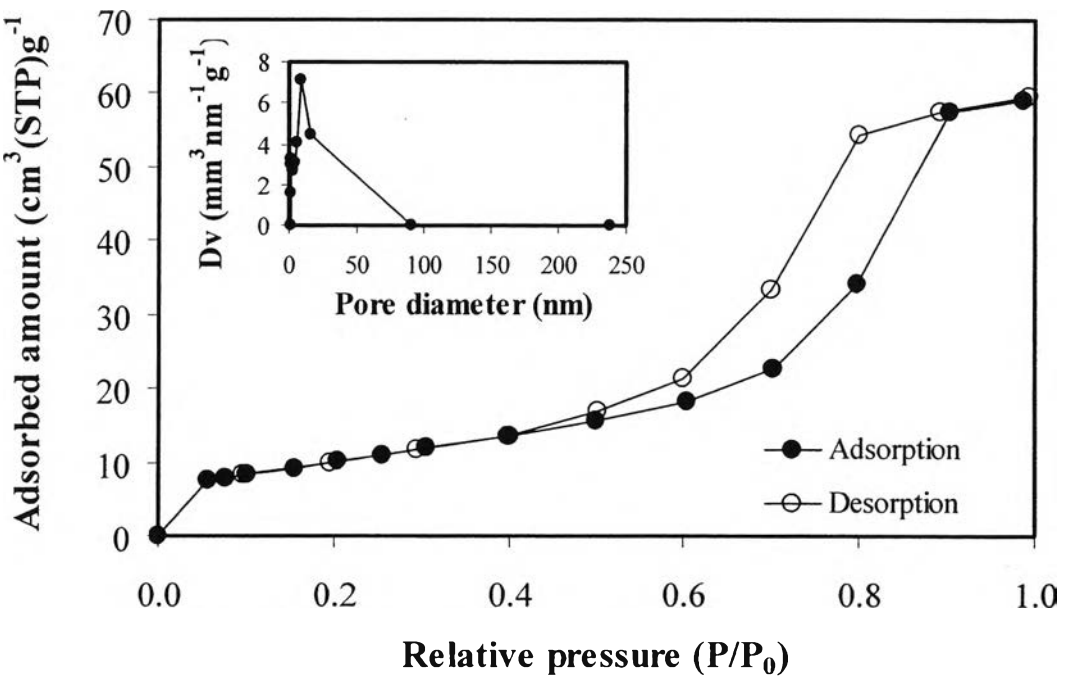

Figure 4.8 N_2 adsorption-desorption isotherms of the 1 mol% RuO_2/TiO_2 (IWI) calcined at 550°C for 4 h (Inset: pore size distribution).

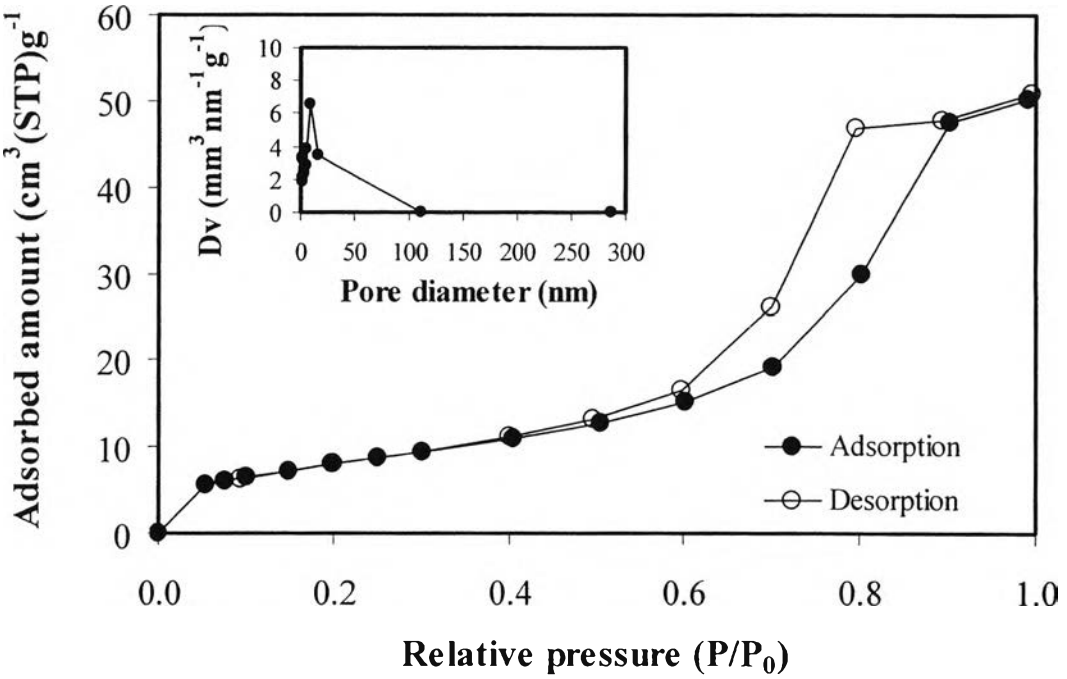

Figure 4.9 N_2 adsorption-desorption isotherms of the 1 mol% RuO_2/TiO_2 (SSSG) calcined at 550°C for 4 h (Inset: pore size distribution).

For the TiO_2 (P-25), SiO_2, and Fe_3O_4, N_2 adsorption-desorption isotherms of all these supports correspond to IUPAC type II pattern (Rouquerol *et al.*, 1999), as depicted in Figure 4.10 to 4.12, respectively. It can be inferred that all these supports exhibited non-mesoporous characteristic because of the absence of both distinct hysteresis loop, observed from the desorption isotherm which was insignificantly different from the adsorption, and adsorption plateau at very high relative pressure, indicating no capillary condensation of N_2 into the pores. Moreover, the pore size distribution of all catalysts, as shown in the inset of Figures 4.10 to 4.12, is quite broad. These results show that the average pore size of all catalysts is quite spacious in average because their pore size distributions are not only present in the mesoporous region (mesoporous size between 2-50 nm) but also mostly exist in the macroporous region (pore diameter > 50 nm). For the Al_2O_3, N_2 adsorption-desorption isotherm exhibits typical IUPAC type IV-like pattern with hysteresis loop, which is characteristic of mesoporous-assembled structure, as shown in Figures 4.13.

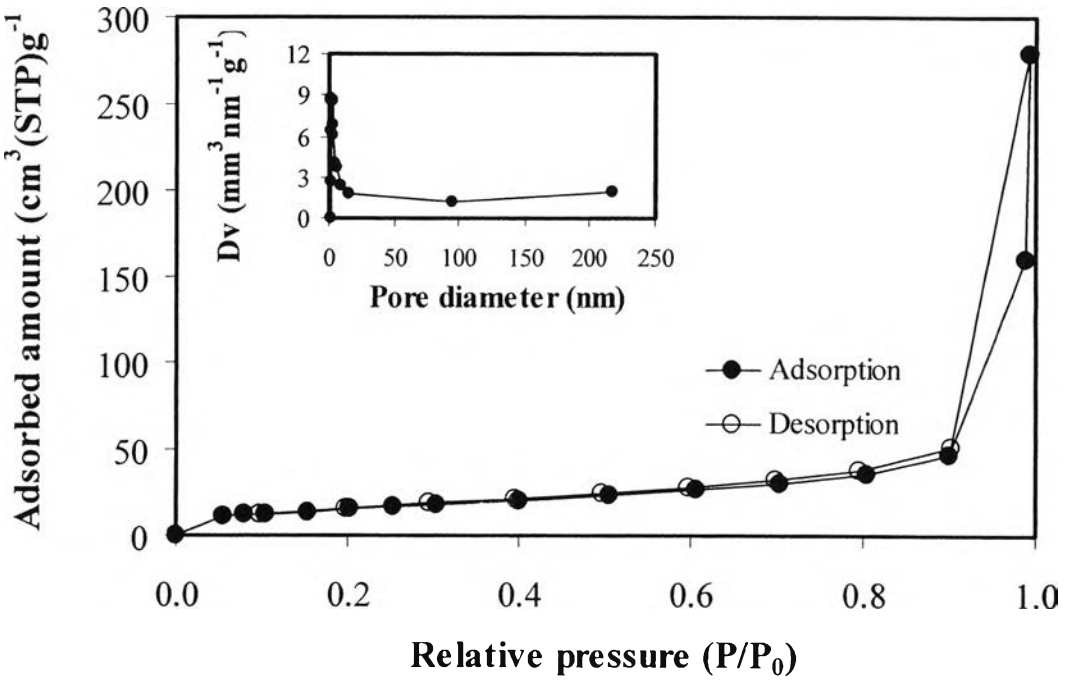

Figure 4.10 N_2 adsorption-desorption isotherms of the TiO_2 (P-25) (Inset: pore size distribution).

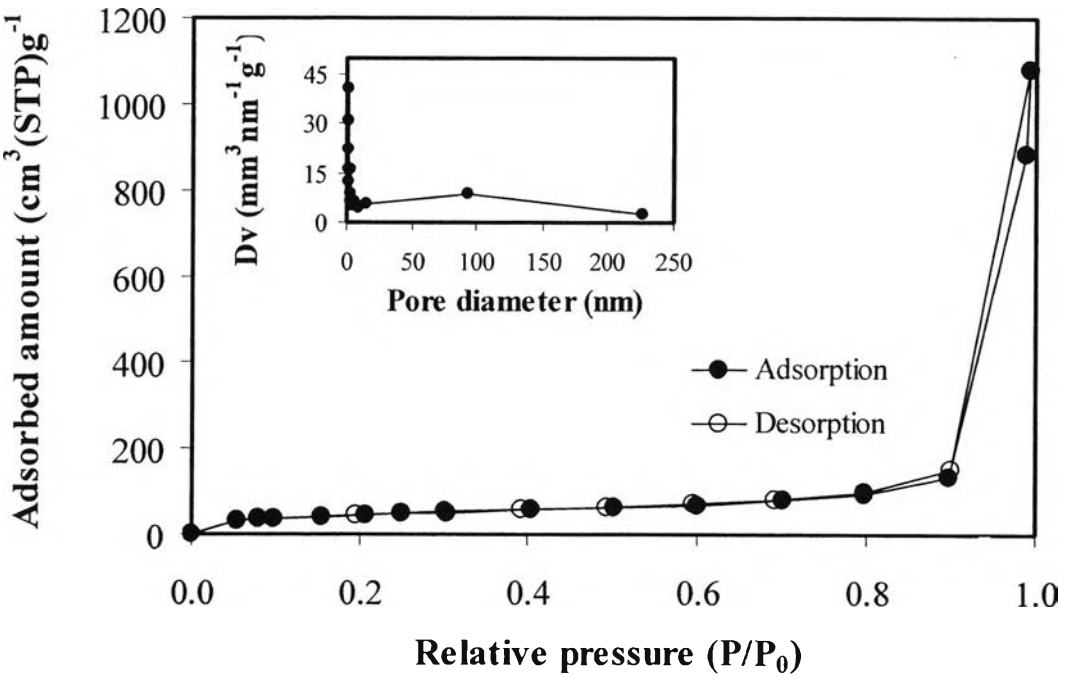

Figure 4.11 N_2 adsorption-desorption isotherms of the SiO_2 (Inset: pore size distribution).

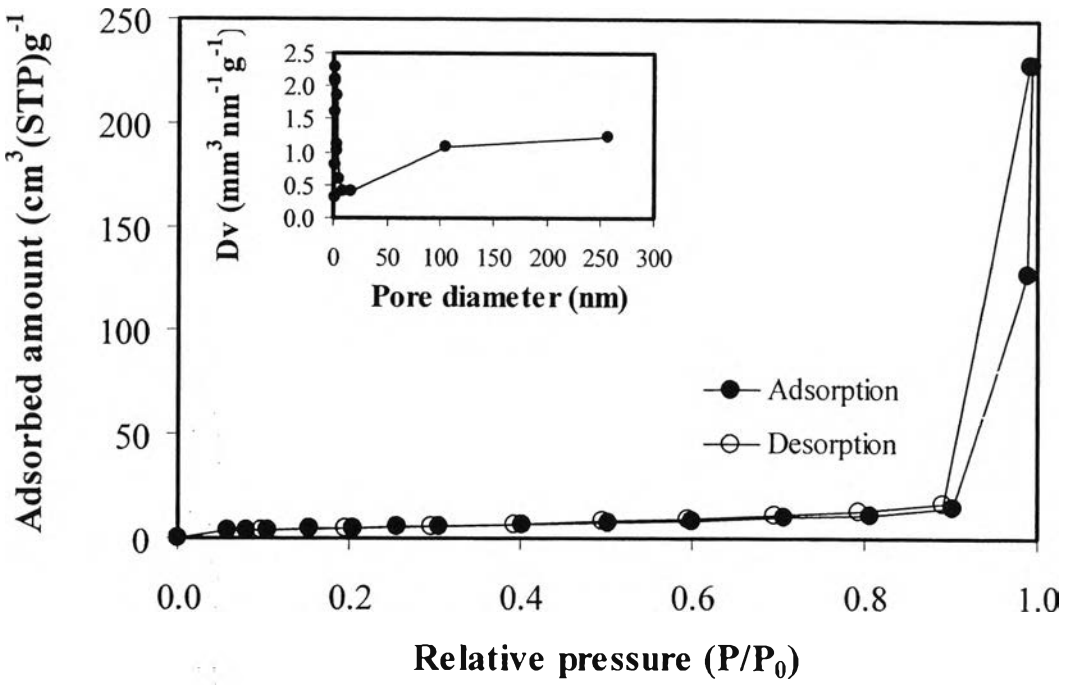

Figure 4.12 N_2 adsorption-desorption isotherms of the Fe_3O_4 (Inset: pore size distribution).

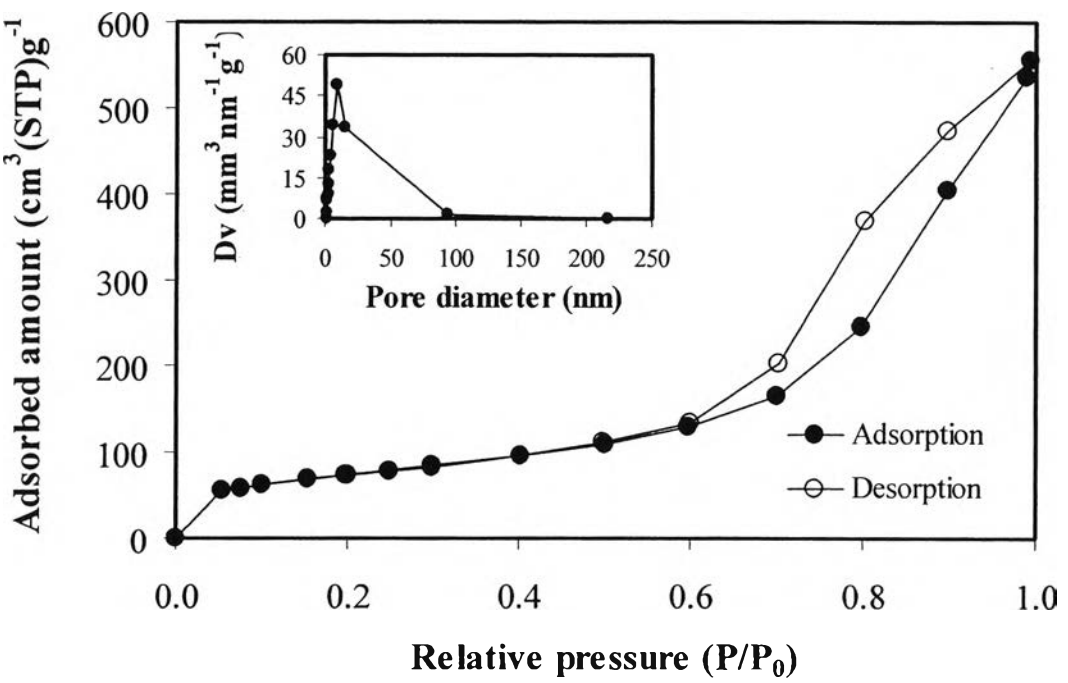

Figure 4.13 N_2 adsorption-desorption isotherms of the Al_2O_3 (Inset: pore size distribution).

The experimental results on textural properties obtained from N_2 adsorption-desorption isotherms, including BET surface area, mean mesopore diameter, and total pore volume, of all catalysts are summarized in Table 4.5. As obviously seen, the surface area of RuO_2/TiO_2 (IWI) decreased from 52.18 to 2.75 $m^2 \cdot g^{-1}$ with increasing calcination temperature from 500 to 700°C, and it decreased from 40.71 to 25.22 $m^2 \cdot g^{-1}$ with increasing calcination time from 3 to 6 h. With increasing calcination temperature, the perceived loss in surface area is explainable to the pore coalescence due to the crystallization of walls separating mesopores. Moreover, the sintering and phase transformation of anatase to rutile phase are concerned (Lin *et al.*, 2007). In addition, this tendency caused an increase in mean mesopore diameter and a decrease in total pore volume of the bulk materials, as expected. With increasing calcination time, the decrease in surface area may be due to pore coalescence in the similar manner to an increase in the calcination temperature, but there is no transformation of anatase to rutile phase (Sreethawong *et* al., 2005). Therefore, it can be inferred that calcination time affects the surface area of RuO_2/TiO_2 (IWI) less than calcination temperature. In the meantime, this also caused a decrease in total pore volume and an increase in mean mesopore diameter.

Since amount of RuO_2 affected the catalytic activity test, RuO_2 loadings on the RuO_2/TiO_2 (IWI) and the RuO_2/TiO_2 (SSSG) were then varied up to 2 mol% to study the optimum loading amount. They were obvious that the surface area gradually decreased from 42.06 to 36.98 $m^2 \cdot g^{-1}$ and from 29.82 to 23.27 $m^2 \cdot g^{-1}$ in the case of IWI and SSSG respectively, with increasing the amount of RuO_2 loaded, plausibly due to the blockage of mesopore dimension with higher RuO_2 content. This subsequently caused the decrease in total pore volume, which was in the similar manner to the surface area. However, the trend of mean pore diameter was relatively different. When 1 mol% RuO_2 was loaded onto the mesoporous-assembled TiO_2 prepared by both IWI and SSSG method, the pore size was increased as previously explained that it could be attributable to the effect of calcination. However, with further increase in the RuO_2 loading amount beyond 1 mol%, the pore size again became decreased to locate at slightly higher level than the unloaded mesoporous-assembled TiO_2. At these high loading amounts, the RuO_2 population may be sufficiently large to reduce the pore dimension. In addition, it is worth noting

that the pore diameter of all loaded catalysts was still in the mesopore region even after passing the loading and two-step calcination processes for RuO_2/TiO_2 (IWI). For the Al_2O_3, the mean pore diameter is 12.75 nm, which exists in the mesoporous region. For the other catalysts, of which isotherms exhibited IUPAC type II pattern, including TiO_2 (P-25), SiO_2, and synthesized Fe_3O_4, the mean pore diameter and total pore volume are always not reported because they contain a large portion of macropore, which possesses very broad pore size distribution with the pore diameter larger than 50 nm.

Table 4.5 Summary of textural properties obtained from N_2 adsorption-desorption results of the TiO_2 (SG), RuO_2/TiO_2 (IWI), RuO_2/TiO_2 (SSSG), TiO_2 (P-25), SiO_2, Al_2O_3, and Fe_3O_4

Catalyst	RuO_2 content (mol%)	Calcination temperature (°C)	Calcination time (h)	BET surface area ($m^2 \cdot g^{-1}$)	Mean mesopore diameter (nm)	Total pore volume ($cm^3 \cdot g^{-1}$)
RuO_2/TiO_2 (IWI)	1	500	4	52.18	9.51	0.13
		550		39.07	10.03	0.09
		600		21.27	11.61	0.06
		700		2.75	-[a]	-[a]
	1	550	3	40.70	9.59	0.10
			5	27.42	10.13	0.07
			6	25.22	10.51	0.06
	0	550	4	42.06	8.51	0.10
	0.5			39.44	9.78	0.10
	1.5			37.12	9.79	0.09
	2			36.98	9.97	0.09

Catalysts	RuO_2 content (mol%)	Calcination temperature (°C)	Calcination time (h)	BET surface area ($m^2 \cdot g^{-1}$)	Mean mesopore diameter (nm)	Total pore volume ($cm^3 \cdot g^{-1}$)
RuO_2/TiO_2 (SSSG)	0.5	550	4	29.82	9.75	0.08
	1			26.02	10.52	0.06
	1.5			24.52	10.41	0.06
	2			23.27	10.49	0.06
TiO_2 (P-25)	-	-	-	55.67	-[a]	-[a]
SiO_2	-	-	-	158.20	-[a]	-[a]
Al_2O_3	-	-	-	260.2	12.75	0.83
Fe_3O_4	-	-	-	17.65	-[a]	-[a]

[a]N_2 adsorption-desorption isotherms correspond to IUPAC type II pattern, indicating the absence of mesoporous structure.

4.2.3 X-ray Diffraction Analysis

The crystalline phases of the catalysts were investigated using XRD analysis. Using RuO_2/TiO_2 (SG) as the catalysts exhibited high potential for catalytic activity of cyclohexene epoxidation as explained later. Therefore, the comparison of XRD patterns of 1 mol% RuO_2/TiO_2 (IWI) with different calcination temperatures are depicted in Figure 4.14. The dominant peak of RuO_2 at 2θ of about 28.1 and 35.1° which represent the indices of (110) and (101) planes respectively could not be observed, presumably due to the combination of its low content, high dispersion degree, and small particle size. The main peaks of 1 mol% RuO_2/TiO_2 (IWI) at 2θ of 25.4, 37.9, 48.1, 53.9, and 55.3°, which represent the indices of (101), (004), (200), (105), and (211) planes respectively, are ascribed to structure of anatase TiO_2. Moreover, it can be seen that at calcination temperature of 500°C, the crystaliization to anatase phase is not fully developed in comparison with the calcination temperature of 550 and 600°C, of which the peak intensity of anatase phase greatly increases. Although the calcination temperature of 550 and 600°C is determined as the highest limit for yielding well-crystalline pure anatase phase, calcination temperature of 600°C is the starting point of phase transformation from anatase to rutile phase since approximately 5% rutile content was observed. All calculated values of rutile ratio (W_R) in terms of weight fraction are presented in Table 4.7. The rutile ratio is estimated from XRD intensity data by using Eq. (4.1) and (4.2) (Spurr and Myers, 1957).

$$W_R = [1 + 0.8I_A/I_R]^{-1} \qquad (4.1)$$

$$W_A = 1 - W_R \qquad (4.2)$$

where I_A and I_R represent integrated intensities of anatase (101) and rutile (110) diffraction peaks respectively, and W_A and W_R represent phase composition of anatase and rutile, respectively. At the calcination temperature 700°C, partial phase transformation from anatase to rutile was observed, resulting in combination between anatase and rutile phases with approximately 62% rutile content. The occurrence of the dominant peaks at 2θ of about 27.4, 36.1, 41.2, 54.2, and 56.8°, which correspond to the indices of (110), (101), (111), (211), and (220) planes respectively, indicates that the rutile phase becomes the main phase in the 1 mol% RuO_2/TiO_2 (IWI) calcined at this temperature. In addition, the results also reveal that with

increasing calcination temperature, the larger TiO_2 crystallite size was obtained as shown in Table 4.6.

Subsequently, since amount of RuO_2 affected the catalytic activity test, the comparison of XRD patterns of RuO_2/TiO_2 (IWI) and RuO_2/TiO_2 (SSSG) calcined at 550°C for 4 h with different amount of RuO_2 loaded are depicted in Figure 4.15 and 4.16, respectively. For RuO_2/TiO_2 (IWI), although amounts of RuO_2 loaded increased, the loaded mesoporous-assembled TiO_2 still maintained highly crystalline anatase structure and crystallite size of the catalysts was relatively unchanged of about 21 nm as included in Table 4.6. In the case of RuO_2/TiO_2 (SSSG) still maintained highly crystalline both anatase and rutile structure and crystallite size of the both anatase and rutile phase was relatively unchanged of about 20 nm and 33 nm respectively, as included in Table 4.6.

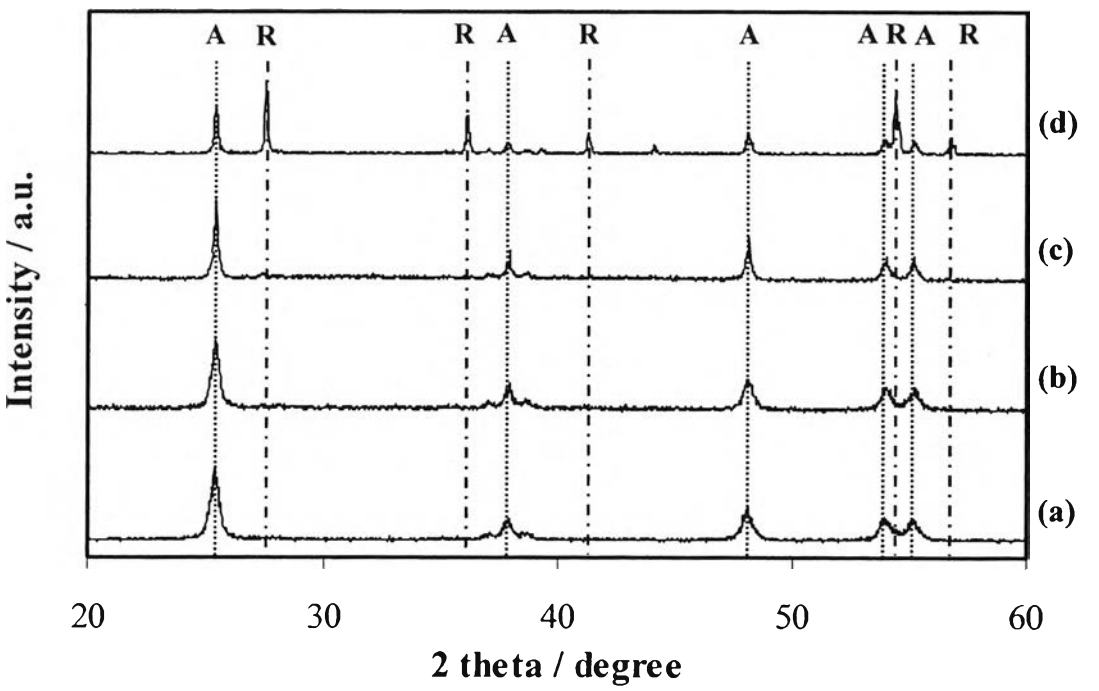

Figure 4.14 XRD patterns of 1 mol% RuO_2/TiO_2 (IWI) calcined for 4 h with different calcination temperatures: (a) 500°C, (b) 550°C, (c) 600°C, and (d) 700°C (A: Anatase, R: Rutile).

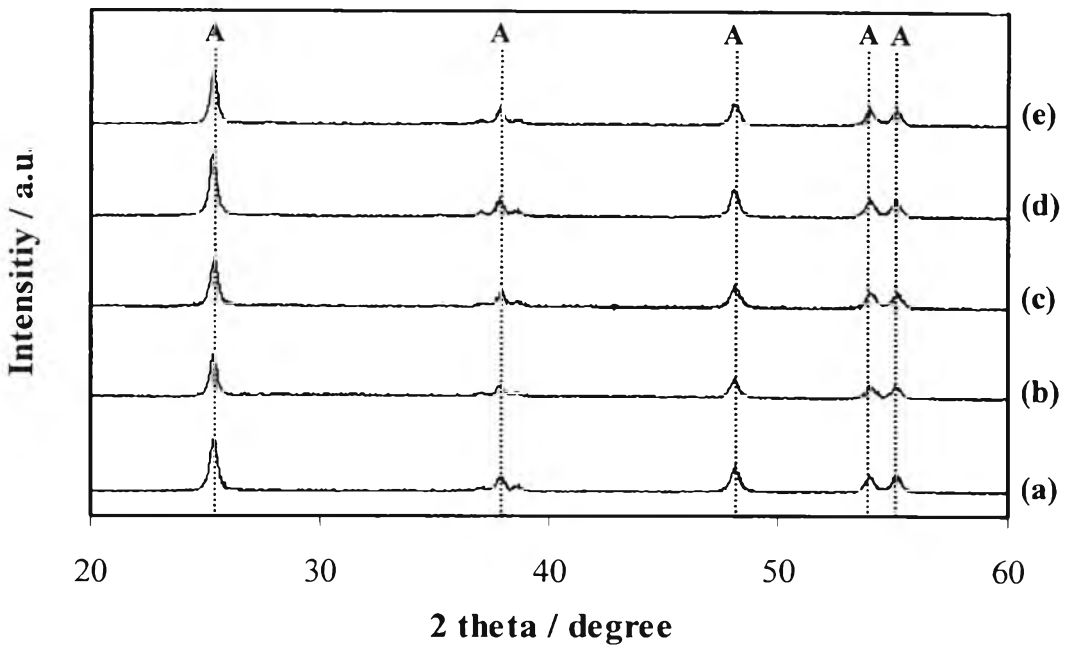

Figure 4.15 XRD patterns of RuO_2/TiO_2 (IWI) calcined at 550°C for 4 h with different RuO_2 amount: (a) unloaded, (b) 0.5 mol%, (c) 1 mol%, (d) 1.5 mol%, and (e) 2 mol% (A: Anatase, R: Rutile).

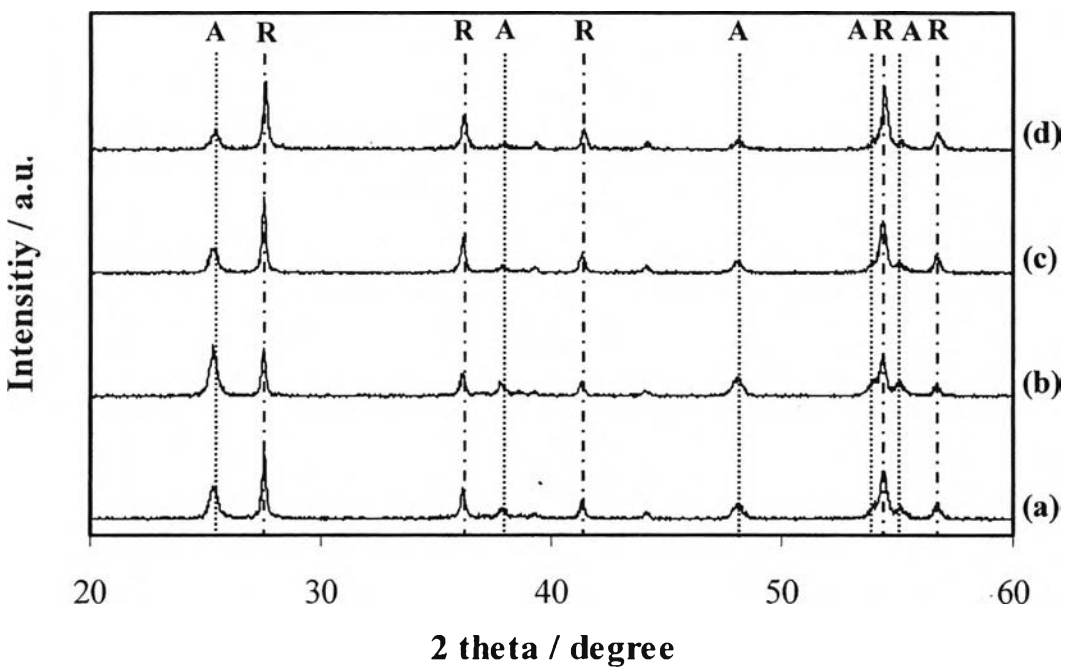

Figure 4.16 XRD patterns of RuO_2/TiO_2 (SSSG) calcined at 550°C for 4 h with different RuO_2 amount: (a) 0.5 mol%, (b) 1 mol%, (c) 1.5 mol%, and (d) 2 mol% (A: Anatase, R: Rutile).

Table 4.6 Summary of XRD analysis of the RuO_2/TiO_2 (IWI) and RuO_2/TiO_2 (SSSG) (A: Anatase, R: Rutile)

Catalyst	RuO_2 content (mol%)	Calcination temperature (°C)	Calcination time (°C)	Phase from XRD Pattern	Rutile ratio (W_R)	Crystallite size (nm)	
						Anatase (101)	Rutile (110)
RuO_2/TiO_2 (IWI)	1	500	4	A	-	17.15	-
		550		A	-	21.49	-
		600		A+R	0.05	28.08	16.09
		700		A+R	0.62	35.35	41.09
RuO_2/TiO_2 (IWI)	0	550	4	A	-	20.46	-
	0.5			A	-	21.32	-
	1.5			A	-	21.78	-
	2			A	-	21.78	-
RuO_2/TiO_2 (SSSG)	0.5	550	4	A+R	0.55	20.40	33.04
	1			A+R	0.61	20.61	33.17
	1.5			A+R	0.76	20.77	34.15
	2			A+R	0.81	20.94	34.45

4.2.4 TEM Analysis

The information about morphological structure and particle sizes of RuO_2 and TiO_2 nanoparticles could be obtained by TEM analysis. As a representative, TEM image of 1 mol% RuO_2/TiO_2 (IWI) calcined at 550°C for 4 h shown in Figure 4.17 demonstrated the formation of nanocrystalline TiO_2 aggregates composed of three-dimensional disordered primary nanoparticles. RuO_2 was observed as deposited particles dispersed on TiO_2 particles, as confirm by the EDX elemental point mapping. The observed TiO_2 particle sizes of 21-25 nm were consistent with the crystallite size estimated from XRD analysis, elucidating that each grain corresponds in average to a single crystallite. In the same manner, the particle size of the RuO_2 single crystalline was approximately 4-5 nm with some aggregations. In addition, TEM image of 1 mol% RuO_2/TiO_2 (SSSG) calcined at 550°C for 4 h shown in Figure 4.18 also indicated the formation of nanocrystalline TiO_2. The particle size of RuO_2 and TiO_2 was observed to be in the range of 2-3 nm and 15-20 nm, respectively. The observed particle size of TiO_2 is in good accordance with the crystallite size calculated from the XRD analysis, signifying that each grain can be considered as a single crystallite. Consequently, from N_2 adsorption-desorption, XRD analysis, and TEM analysis, the mesoporous structure of the synthesized TiO_2 nanocrystal can be plausibly originated from the pore formed between nanocrystalline TiO_2 particles due to their aggregated assembly.

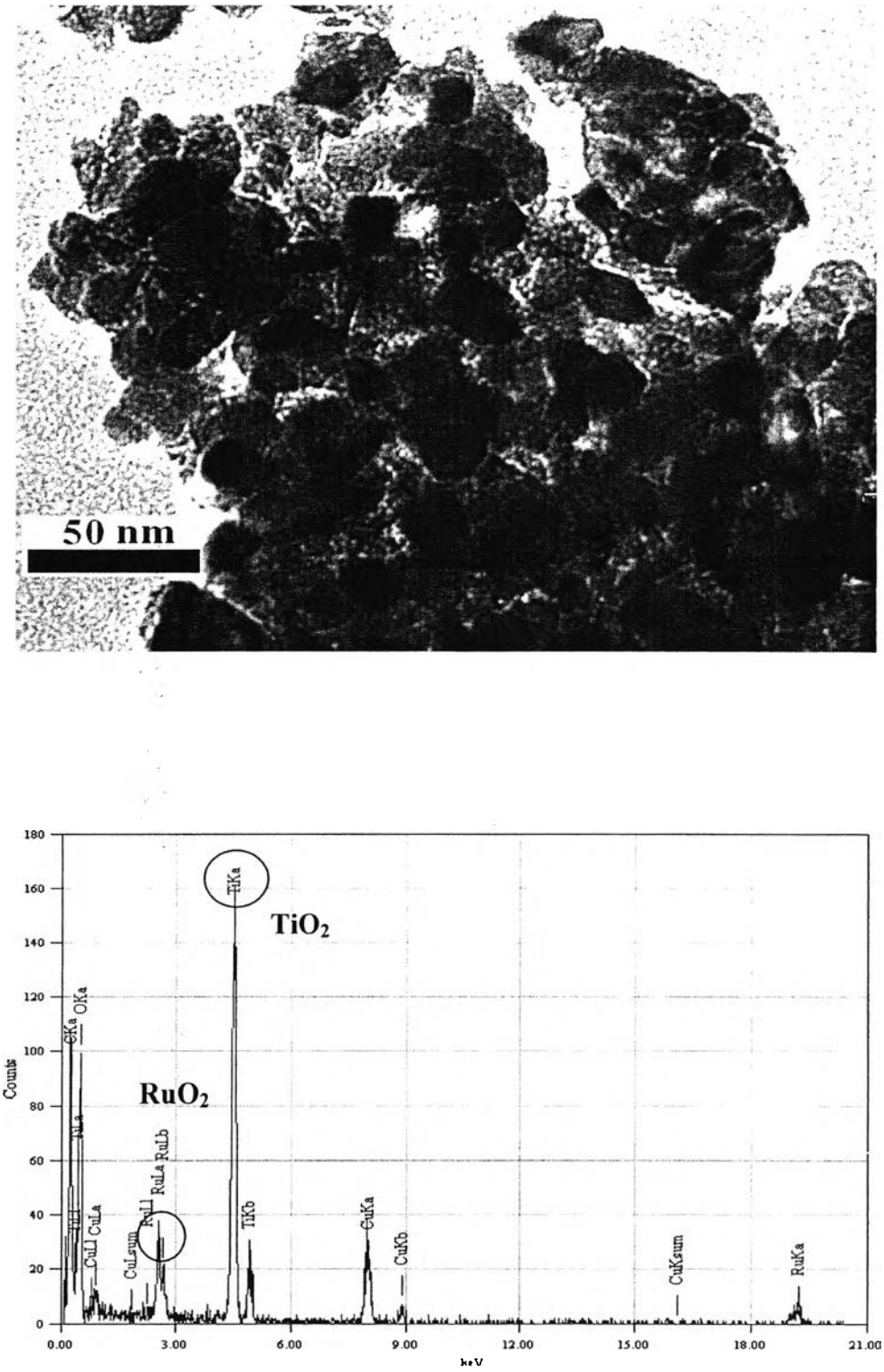

Figure 4.17 TEM image and EDX elemental point mapping of 1mol% RuO_2/TiO_2 (IWI) calcined at 550°C for 4 h.

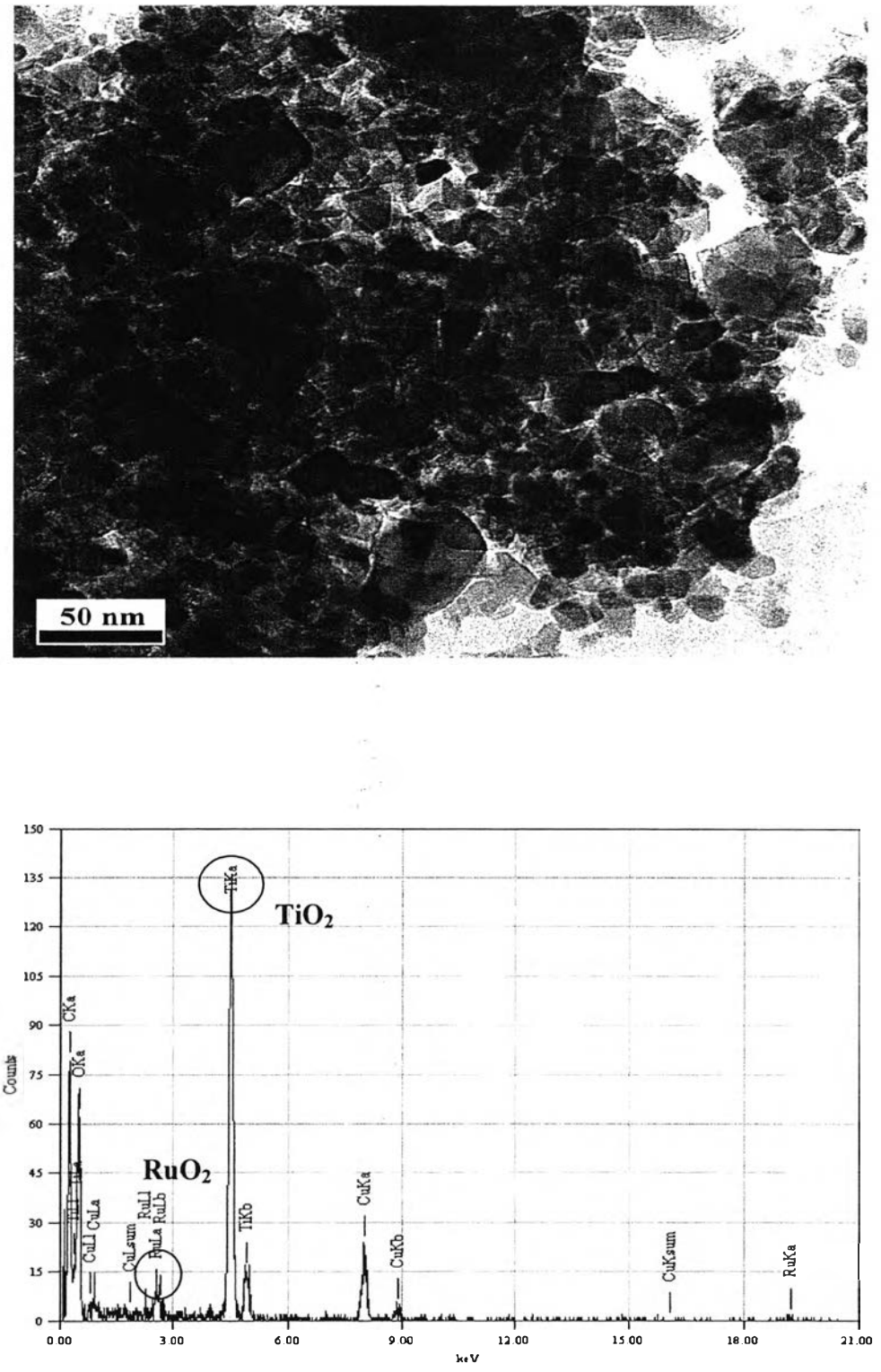

Figure 4.18 TEM image and EDX elemental point mapping of 1mol% RuO_2/TiO_2 (SSSG) calcined at 550°C for 4 h.

4.3 Catalytic Activity of Cyclohexene Epoxidation

4.3.1 Blank Test

Epoxidation of cyclohexene was initially studied with control experiment in order to determine the effect of catalysts, oxidants, and atmospheric air. In this section, the blank tests were done with 3 different cases; 1) no catalysts, 2) no oxidants, and 3) no both catalysts and oxidants. The results of cyclohexene conversion and product selectivity for all cases are summarized in Table 4.7. It was observed that the reaction scarcely occurred in the case of no oxidant (case 2 and 3). On the other hand, in case of no catalyst present in the system, the results from product determination reveal that the auto-oxidation of cyclohexene to form cyclohexene oxide and 2-cyclohexen-1-ol but with relatively low cyclohexene conversion (= 7.54% after 5 h of reaction) was observed. Therefore, the main products are cyclohexene oxide and 2-cyclohexen-1-ol with similar amount. This is plausibly owing to the strong oxidizing power of H_2O_2, where it reacts with *tert*-butanol to initially form the in situ generated *tert*-butyl hydroperoxide, which functions as a major source of the initiator and is then thermally decomposed to generate active free radicals for auto-oxidation reaction. These free radicals then react with cyclohexene to form organic compound radical, which is propagated through the reaction with molecular O_2 to form intermediate peroxide radical. Due to the low stability of this intermediate radical at the temperatures required for the reaction, it undertakes homolytic decomposition to afford nonradical products, mainly cyclohexene oxide and 2-cyclohexen-1-ol. Additionally, cyclohexene inevitably undergoes the oxidation in allylic position with the initiator radical, i.e. *tert*-butoxy radical to form 2-cyclohexen-1-ol, which is also further oxidized to 2-cyclohexen-1-one. Meanwhile, cyclohexene oxide also unavoidably suffers ring opening by hydrolysis because of the present of water produced from the reaction to form *trans*-1,2-cyclohexanediol.

Table 4.7 Control experiment by 1) no catalysts, 2) no oxidant, and 3) no both catalyst and oxidant for cyclohexene epoxidation. Reaction conditions: cyclohexene 30 mmol; *tert*-butanol 30 ml; reaction temperature 70°C

	Case 1 no catalyst		**Case 2 no oxidant**		**Case 3 no catalyst and oxidant**	
	3 h	**5 h**	**3 h**	**5 h**	**3 h**	**5 h**
Conversion, %	2.25	7.54	1.10	2.23	0.64	1.16
Selectivity, %						
Cyclohexene oxide	45.61	49.27	0	0	0	0
2-Cyclohexen-1-ol	33.30	31.39	0	0	0	0
2-Cyclohexen-1-one	7.28	7.38	0	0	0	0
trans-1,2-Cyclohexanediol	5.56	6.19	0	0	0	0
Others (unknown)	8.25	5.17	100	100	100	100

4.3.2 Effect of Catalysts

Five oxide catalysts—TiO_2 (SG) calcined at 500°C, TiO_2 (P-25), SiO_2, Al_2O_3, and Fe_3O_4—were separately tested at the same experimental conditions for cyclohexene epoxidation. In this study, it was found that all catalysts were active for the cyclohexene epoxidation with hydrogen peroxide as an oxidant because there is the change of cyclohexene conversion. The catalytic activity in terms of cyclohexene conversion and product selectivity are given in Figure 4.19.

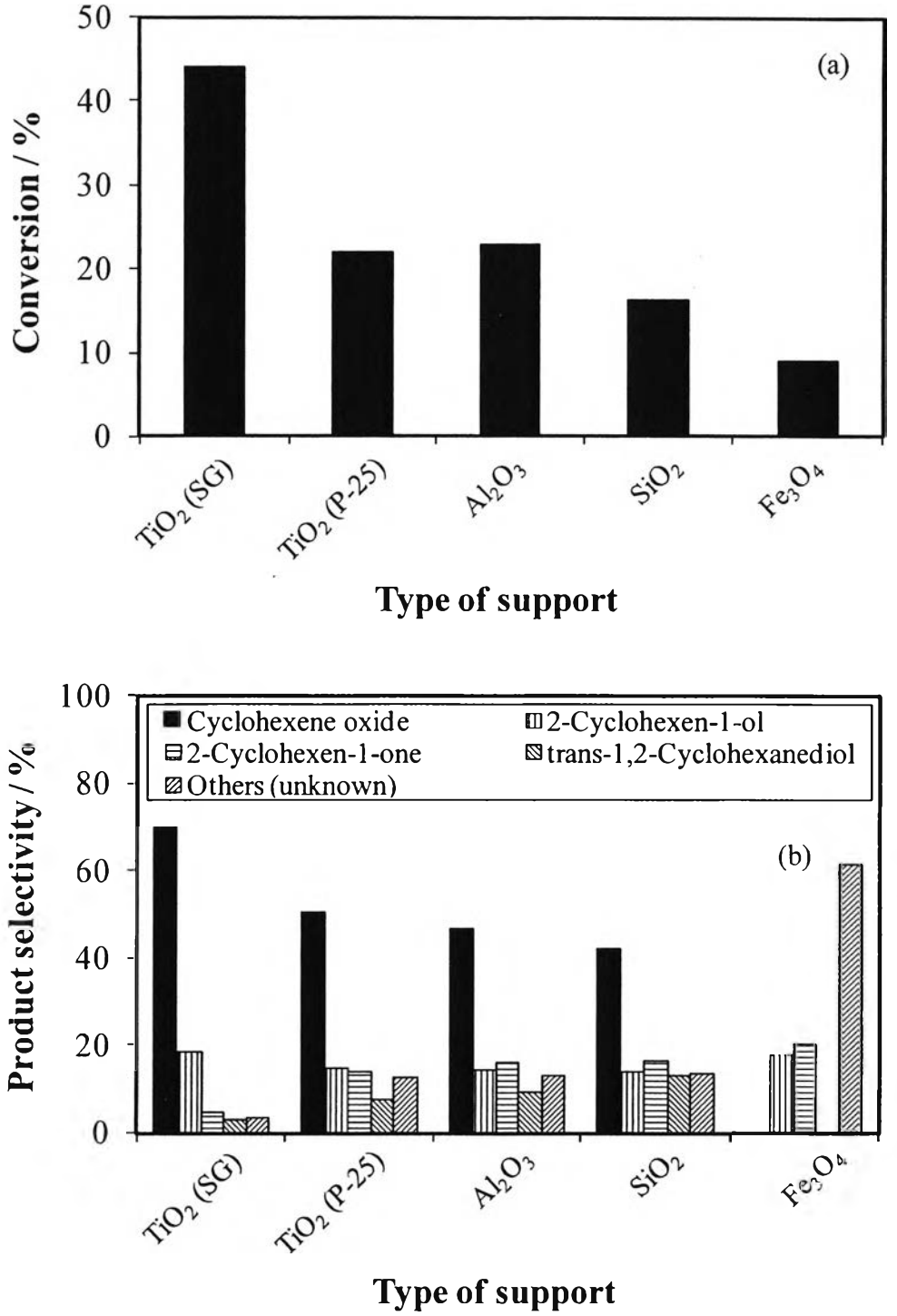

Figure 4.19 Cyclohexene epoxidation catalyzed by TiO_2 (SG) calcined at 500°C, TiO_2 (P-25), SiO_2, Al_2O_3, and Fe_3O_4: (a) cyclohexene conversion and (b) product selectivity. Reaction conditions: cyclohexene 30 mmol; *tert*-butanol 30 mmol; H_2O_2 30 mmol; catalyst 0.5 g; reaction temperature 70°C; reaction time 5 h.

It was observed that TiO_2 (SG) gave the highest of cyclohexene conversion (44.14%), approximately two folds higher than TiO_2 (P-25) and Al_2O_3. The cyclohexene oxide selectivity in the case of TiO_2 (SG) was also the highest compared with other catalysts. The product selectivity of all catalysts, except TiO_2 (SG), was rather varied with not only low cyclohexene oxide selectivity but also very high 2-cyclohexen-1-one selectivity. According to these preliminary results, the TiO_2 (SG) has superior catalytic performance to other supports in the terms of both conversion and desired product selectivity because TiO_2 (SG) possesses narrow pore size distribution which advantageously makes it a versatile in this reaction. Although possessing higher surface area than the TiO_2 (SG), the SiO_2 has no mesoporosity, so the mesoporosity contained in the synthesized TiO_2 seems to play much more significant role in enhancing reactant accessibility and surface reaction through the mesoporous structure and also to play significant role more significant role in enhancing reactant accessibility than Al_2O_3. In case of the TiO_2 (P-25), the absence of mesopore with low surface area as well as the presence of rutile phase (Sreethawong *et al.*, 2005) can disadvantageously influence on the observed low catalytic performance. Even if the effect of rutile phase is not yet clearly understood, the less degree of hydroxylation (i.e. less number of surface hydroxyl groups) of the rutile structure rather than the anatase one may be considered as a probable drawback in cyclohexene epoxidation. Moreover, Fe_3O_4 was the least active catalyst for cyclohexene epoxidation when compared with the other catalysts since Fe_3O_4 was not mesoporosity as well as low surface area, so there was not cyclohexene oxide which is main product occurred. Therefore, it can be inferred that the TiO_2 (SG) is quite a promising catalyst for cyclohexene epoxidation.

4.3.3 Effect of Calcination Temperature

Further study was focused on the effect of calcination temperature to catalytic activity of 1 mol% RuO_2/TiO_2 (IWI). From literature, it was clearly seen that the effect of metal oxide additives loaded onto the TiO_2 (SG) intended to achieve the improvement of the catalytic performance. In addition, it was found that RuO_2 loaded onto TiO_2 (SG) gave the highest of both cyclohexene conversion and cyclohexene oxide selectivity accompanying with relatively low 2-cyclohexen-1-ol selectivity when compared with CoO_x-loaded, NiO_x-loaded, and FeO_x-loaded. Namely, RuO_2/TiO_2 (IWI) is a promising catalyst in the investigated cyclohexene epoxidation (Sreethawong *et al.*, 2005). Moreover, α-TiMAS, which M is transition metals, i.e. Ru(III), Cu(II), and Cr(III), is the best catalyst for the cyclohexene epoxidation when using Ru(III) as the transition metals (Khare and Shrivastava, 2004). Therefore, RuO_2 taken to improve cyclohexene oxide production was then used as the metal oxide additive in this study. The cyclohexene conversion and product selectivity of 1 mol% RuO_2/TiO_2 (IWI) calcined for 4 h with different calcination temperatures are shown in Figure 4.20. It can be clearly observed that 1 mol% RuO_2/TiO_2 (IWI) calcined at 550°C for 4 h provided the highest both cyclohexene conversion and cyclohexene oxide selectivity when compared with other calcination temperatures. At the calcination temperature of 500°C, the crystallization to anatase phase of the synthesized catalyst is not fully developed in comparison with the calcination temperature of 550°C. Besides, at the calcination temperature of 600 and 700°C, partial phase transformation from anatase to rutile was observed, resulting in combination between anatase and rutile phases, namely, the presence of rutile phase can disadvantageously influence on the low catalytic performance because the less degree of hydroxyl group of the rutile structure rather than the anatase one.

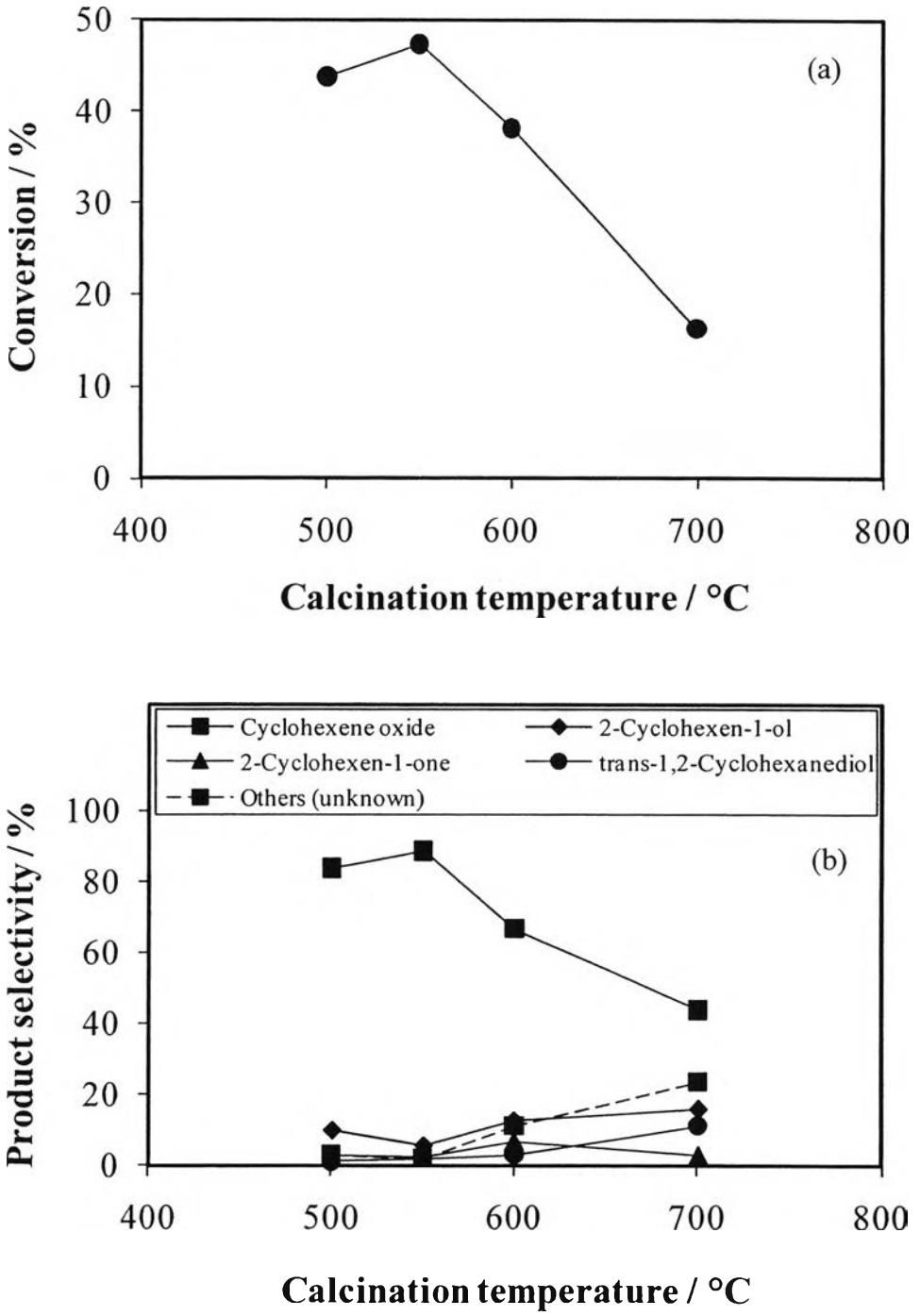

Figure 4.20 Cyclohexene epoxidation catalyzed by 1 mol% RuO_2/TiO_2 (IWI) calcined for 4 h with different calcination temperatures: (a) cyclohexene conversion and (b) product selectivity. Reaction conditions: cyclohexene 30 mmol; *tert*-butanol 30 ml; H_2O_2 30 mmol; catalyst 0.5 g; reaction temperature 70°C; reaction time 5 h.

4.3.4 Effect of Calcination Time

This study was focused on the effect of calcination time to catalytic activity of 1 mol% RuO_2/TiO_2 (IWI) calcined at 550°C (suitable calcination temperature). The cyclohexene conversion and product selectivity of 1 mol% RuO_2/TiO_2 (IWI) calcined at 550°C with different calcination times are shown in Figure 4.21. It can be seen that 1 mol% RuO_2/TiO_2 (IWI) calcined at 550°C for 4 h provided the highest both cyclohexene conversion and cyclohexene oxide selectivity when compared with other calcination times. Although the calcination time of 3 h possesses higher surface area than one, this calcination time may not be sufficient for both complete surfactant template removal and the crystallization to anatase phase. At the calcination time of 5 and 6 h, the catalytic activity decreased. This can be attributed that increasing the calcination time from 4 to 6 caused the amount of OH on the surface decreased from 3.99 to 2.71 OH/g which may be considered as a drawback in this reaction.

4.3.5 Effect of RuO_2 Loading

Since RuO_2/TiO_2 (IWI) calcined at 550°C for 4 h shows the highest both cyclohexene conversion and cyclohexene oxide selectivity, the amount of RuO_2 loaded onto TiO_2 (SG) calcined at 550°C for 4 h (suitable calcination temperature and calcination time) was considered as the main factor needed to be examined prior to further investigations.

4.3.5.1 Effect of mol% RuO_2/TiO_2 (IWI)

The RuO_2 loading amount was studied from 0 to 2 mol% with 0.5 mol% increment, aiming to acquire the catalytic improvement. The cyclohexene conversion and product selectivity over these catalysts are illustrated in Figure 4.22. Although TiO_2 (SG) provided higher cyclohexene conversion than RuO_2/TiO_2 (IWI), RuO_2/TiO_2 (IWI) showed higher cyclohexene oxide selectivity and lower 2-cyclohexen-1-ol selectivity. Unfortunately, the increment in the amount of RuO_2 loaded beyond 1 mol% not only resulted in lower cyclohexene conversion but also lower cyclohexene oxide selectivity and higher undesired product selectivity. These results might be related to their textural properties shown in Table 4.6. As the pore size and pore volume were decreased in some extents when the RuO_2 loading amount

was higher than 1 mol%, the reactant accessibility into the mesoporous structure could be reduced. The less accessible reactants could lead to the lower cyclohexene conversion than that in the case of 1 mol% RuO_2-loaded catalyst. Because more extent of cyclohexene was left in the bulk solution outside the mesoporous reactive surface, it might undergo auto-oxidation more easily to yield higher undesired product contents, corresponding to higher undesired product selectivity.

4.3.5.2 Effect of mol% RuO_2/TiO_2 (SSSG)

RuO_2/TiO_2 (SSSG) calcined at 550°C for 4 h is expected that it was able to accomplish the improvement of the catalytic performance since RuO_2/TiO_2 (SSSG) could be able to help stabilize the mesopore due to inhibiting the coalescence of the TiO_2 nanoparticles. Therefore, the RuO_2 loading amount was then studied from 0 to 2 mol% with 0.5 mol% increment in order to compare with RuO_2/TiO_2 (IWI) calcined at 550°C for 4 h. The cyclohexene conversion and product selectivity over these catalysts are depicted in Figure 4.23. It can be seen that the trend of both cyclohexene conversion and cyclohexene oxide selectivity was in the similar manner to the RuO_2/TiO_2 (IWI). When compared with 1 mol% RuO_2/TiO_2 (IWI), 1 mol% RuO_2/TiO_2 (SSSG) showed lower cyclohexene conversion and cyclohexene oxide selectivity. It can be explained that at the calcination temperature of 550°C, the partial phase transformation from anatase to rutile was observed shown in Figure 4.16, which caused the low catalytic performance. Hence, 1 mol% RuO_2/TiO_2 (IWI) was evaluated as very active cyclohexene epoxidation catalyst in this investigated system.

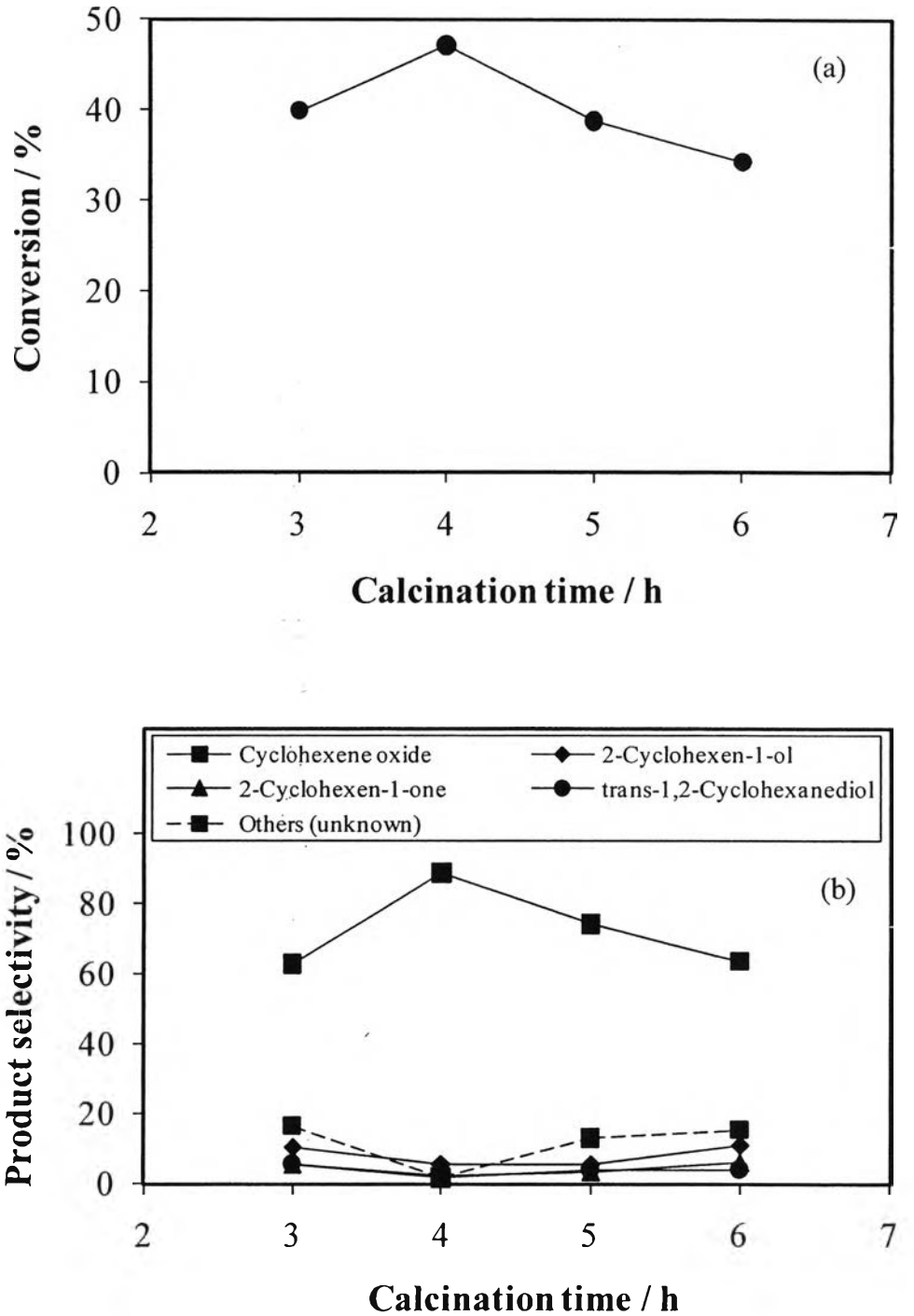

Figure 4.21 Cyclohexene epoxidation catalyzed by 1 mol% RuO_2/TiO_2 (IWI) calcined at 550°C with different calcination times: (a) cyclohexene conversion and (b) product selectivity. Reaction conditions: cyclohexene 30 mmol; *tert*-butanol 30 ml; H_2O_2 30 mmol; catalyst 0.5 g; reaction temperature 70°C; reaction time 5 h.

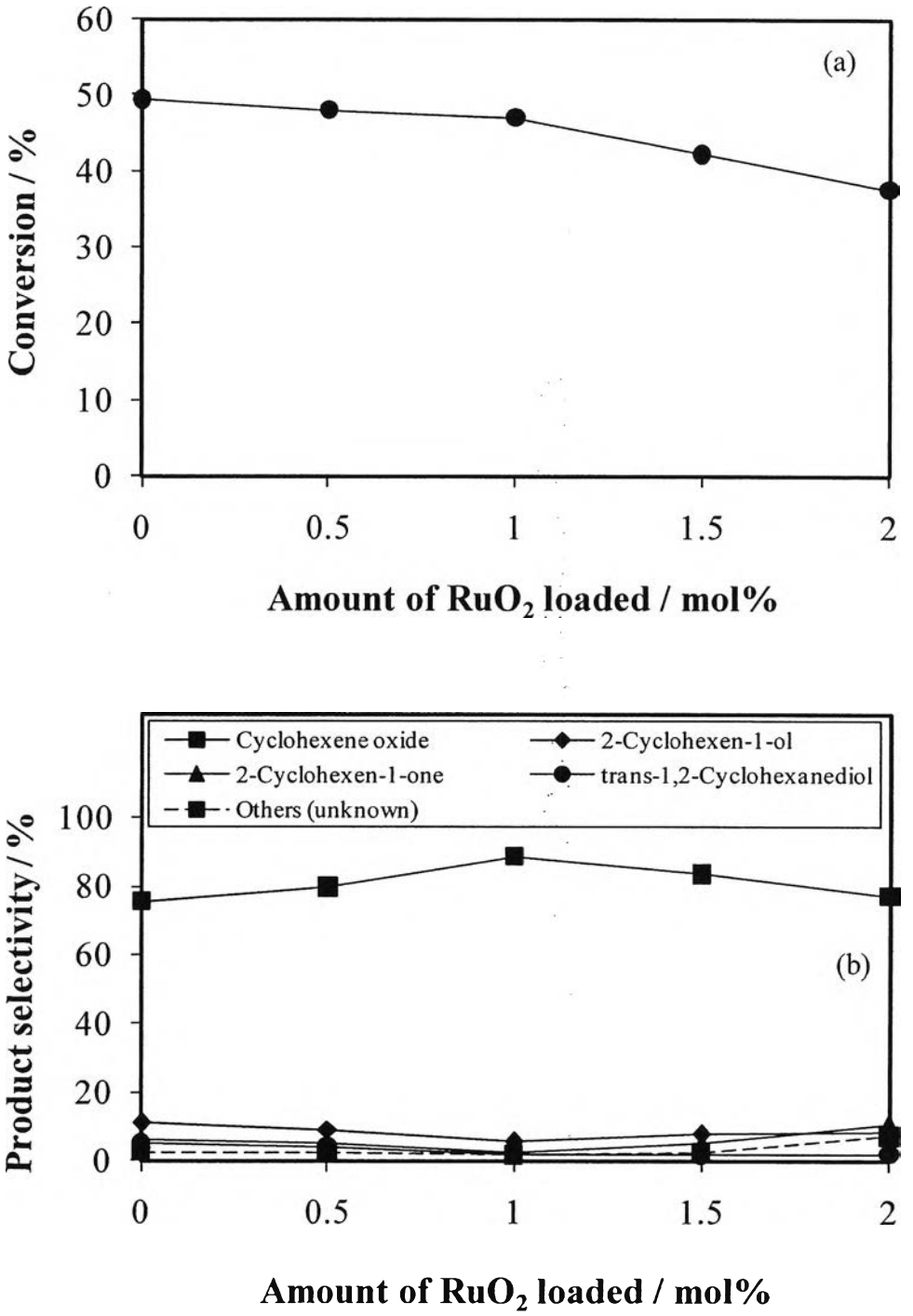

Figure 4.22 Cyclohexene epoxidation catalyzed by RuO_2/TiO_2 (IWI) calcined at 550°C for 4 h with different RuO_2 amount: (a) cyclohexene conversion and (b) product selectivity. Reaction conditions: cyclohexene 30 mmol; *tert*-butanol 30 ml; H_2O_2 30 mmol; catalyst 0.5 g; reaction temperature 70°C; reaction time 5 h.

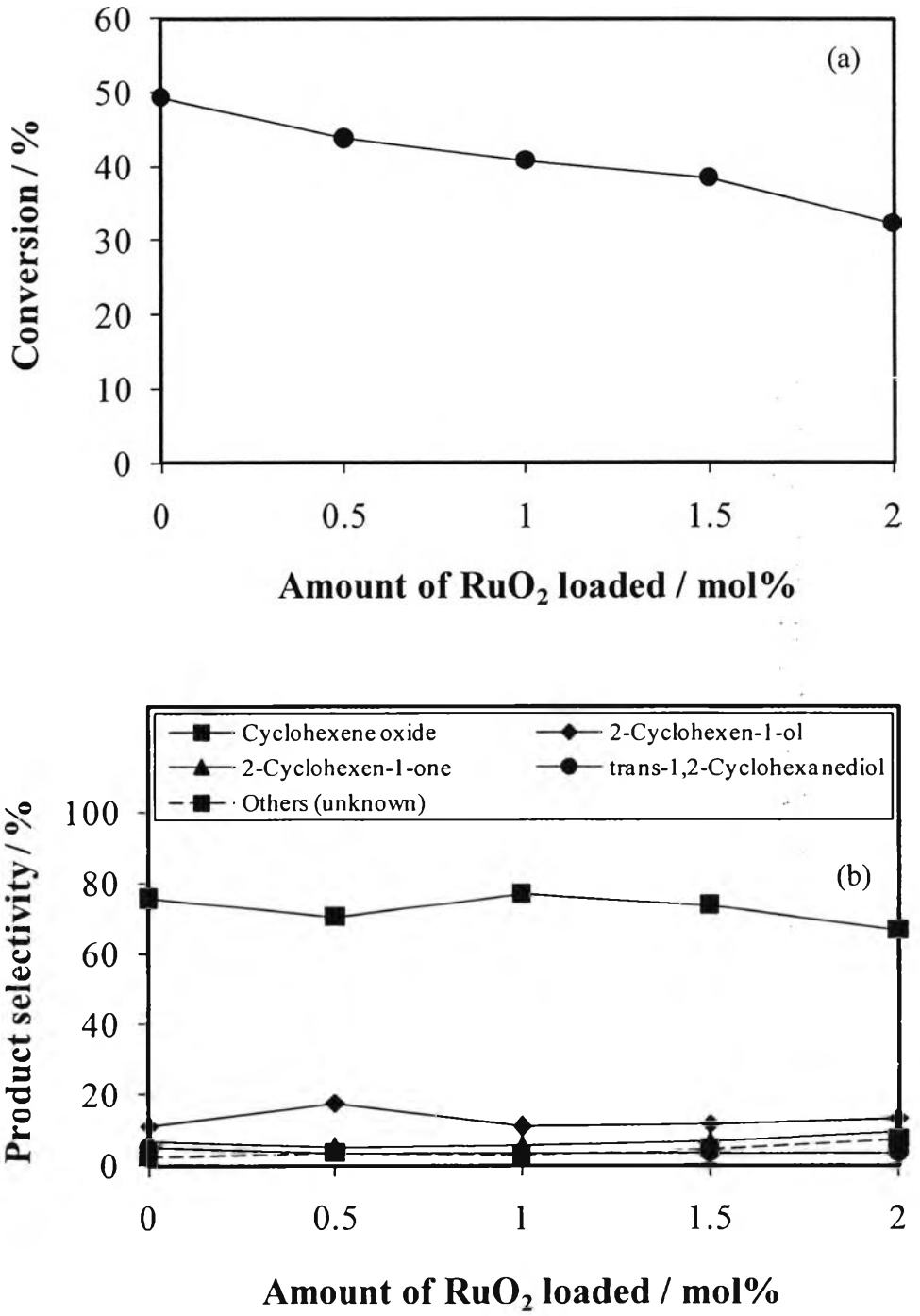

Figure 4.23 Cyclohexene epoxidation catalyzed by RuO_2/TiO_2 (SSSG) calcined at 550°C for 4 h with different RuO_2 amount: (a) cyclohexene conversion and (b) product selectivity. Reaction conditions: cyclohexene 30 mmol; *tert*-butanol 30 ml; H_2O_2 30 mmol; catalyst 0.5 g; reaction temperature 70°C; reaction time 5 h.

4.3.6 Effect of Reaction Parameters

The TiO_2 (SG) method exhibited high potential to be used as cyclohexene epoxidation catalyst, compared with TiO_2 (P-25), SiO_2, Al_2O_3, Fe_3O_4. In addition, the RuO_2 loading by IWI method significantly enhanced both the cyclohexene conversion and cyclohexene oxide selectivity of TiO_2 (SG), exhibiting the optimum loading content of 1 mol%. Since high cyclohexene oxide selectivity has been focused as a target for developing catalyst, the 1 mol% RuO_2/TiO_2 (IWI) calcined at 550°C for 4 h has been taken to improve cyclohexene oxide production by further optimization of reaction conditions.

4.3.6.1 Effect of Reaction Temperature

The effect of reaction temperature in cyclohexene epoxidation using H_2O_2 as an oxidant was initially studied in the range from 50 to 80°C. The results of the effect of the reaction temperature are shown in Figure 4.24. It was obviously seen that over 70°C, the reaction seemed to be uncontrollable and too severe because the reflux could not appropriately compensate with the continuously generated gaseous species which occurred from decomposition of *tert*-butanol and cyclohexene because reaction temperature close by the boiling point of these substances. Moreover, it was observed that cyclohexene conversion drastically decreased and cyclohexene oxide selectivity moderately decreased with decreasing the reaction temperature from 70°C to 50°C. On the other hand, the selectivities to the other two undesired products (2-cyclohexen-1-ol, and 2-cyclohexen-1-one) increased. Therefore, this can be inferred that the reaction temperature of 70°C is an optimum point to yield the highest cyclohexene oxide selectivity under the controllable reaction temperature interval.

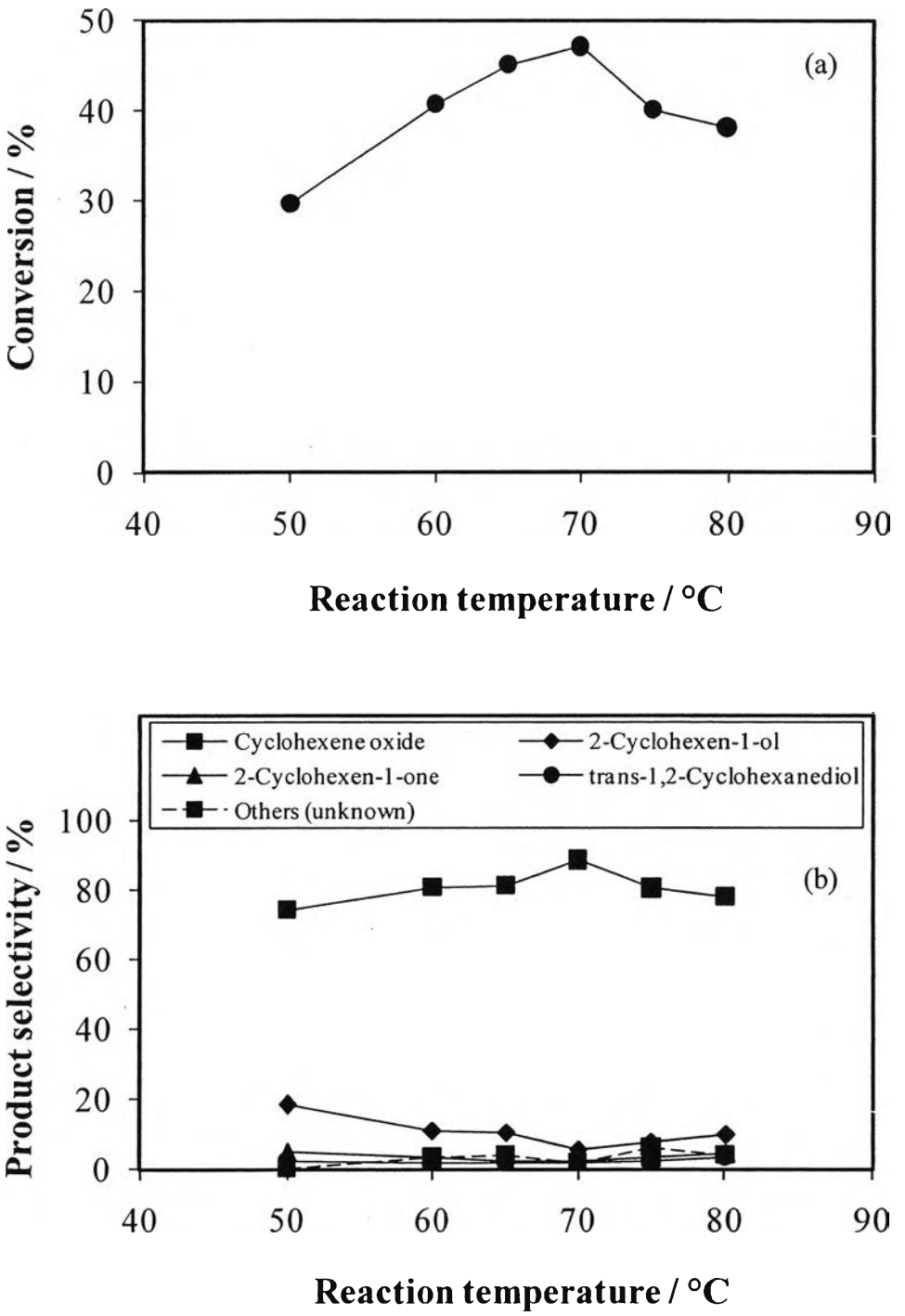

Figure 4.24 Effect of reaction temperature on cyclohexene epoxidation catalyzed by 1 mol% RuO_2/TiO_2 (IWI) calcined at 550°C for 4 h: (a) cyclohexene conversion and (b) product selectivity. Reaction conditions: cyclohexene 30 mmol; *tert*-butanol 30 ml; H_2O_2 30 mmol; catalyst 0.5 g; reaction time 5 h.

4.3.6.2 Effect of Catalyst Amount

The effect of the amount of catalyst, RuO_2/TiO_2 (IWI), in cyclohexene epoxidation was further optimized by maintaining the reaction temperature at 70°C. The catalyst amount was increased up to 0.80 g under the identical reaction conditions. The effect of catalyst amount is shown in Figure 4.25. It can be seen that cyclohexene conversion severely increased with increasing the catalyst amount but after catalyst amount of 0.50 g cyclohexene conversion slightly increased. However, by considering the cyclohexene oxide selectivity, the catalyst amount of 0.50 g provided the highest cyclohexene oxide selectivity of 88.50, while selectivity of other products was a minimum (2-cyclohexen-1-ol = 5.50%, and 2-cyclohexen-1-one = 2.45%). Similar observation has also been reported in case of α-titanium arsenate using *tert*-butyl hydroperoxide as an oxidant (Khare and Shrivastava, 2004), in which the optimum catalyst amount that yielded maximum cyclohexene oxide selectivity and minimum 2-cyclohexen-1-ol and 2-cyclohexen-1-one selectivities was reported. However, when the applied catalyst amount was larger, it was mentioned that the complete absorption of water produced during the reaction can assist avoid the ring-opening of the epoxide from hydrolysis, so *trans*-1,2-cyclohexanediol occurring from catalyst amount of 0.80 g was less than compared with other catalyst contents (Mandelli *et al.*, 2001). From these results, the optimum conditions for the reaction temperature and catalyst amount are 70°C and 0.50 g, respectively since providing the highest cyclohexene oxide selectivity.

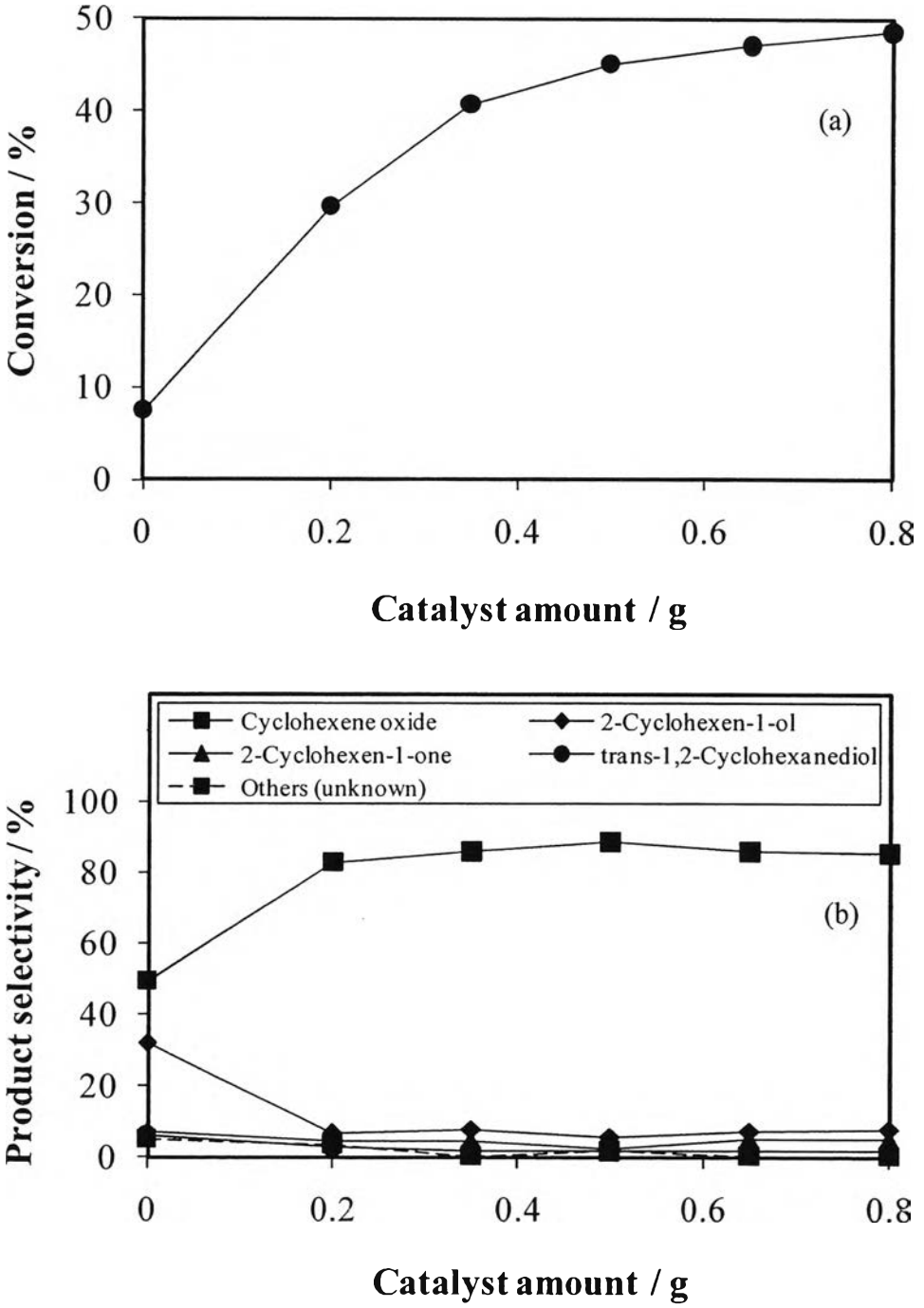

Figure 4.25 Effect of catalyst amount on cyclohexene epoxidation catalyzed by 1 mol% RuO_2/TiO_2 (IWI) calcined at 550°C for 4 h: (a) cyclohexene conversion and (b) product selectivity. Reaction conditions: cyclohexene 30 mmol; *tert*-butanol 30 ml; H_2O_2 30 mmol; reaction temperature 70°C; reaction time 5 h.

4.3.6.3 Effect of Hydrogen Peroxide-to-Cyclohexene Ratio

The concentration of H_2O_2 was also another significant parameter affecting the cyclohexene oxide selectivity to be further optimized. By fixing the substrate (cyclohexene) amount constant, the effect of H_2O_2 amount was studied over a wide range of H_2O_2-to-cyclohexene molar ratio from 0.1 to 6.67 with the RuO_2/TiO_2 (IWI) (note that the previously described results were based on the ratio of 1). Figure 4.26 represents the cyclohexene conversion and product selectivities at different H_2O_2-to-cyclohexene ratios. As obviously seen, the cyclohexene conversion is almost independent of the H_2O_2-to-cyclohexene ratio in all cases at approximately 35-45% over the entire range. However, it is interestingly found that the cyclohexene oxide selectivity dramatically decreased after leveling off beyond the ratio of 1 but the 2-cyclohexen-1-ol selectivity significantly increased, which noticeably declined until becoming almost unchanged at an identical value. In the meantime, the 2-cyclohexen-1-one and *trans*-1,2-cyclohexandiol selectivity was comparatively low only around 5-10% and 1-5%, respectively and its change in selectivity was relatively much less than that of other products. Therefore, the H_2O_2-to-cyclohexene ratio of 1 is sufficient to attain the highest of both cyclohexene conversion and cyclohexene oxide selectivity. At the H_2O_2-to-cyclohexene ratio higher than optimum value of 1, large amount of H_2O_2 might be left in the solution phase, being able to react with cyclohexene via chain free radical reaction upon auto-oxidation pathway. In conjunction with the surface epoxidation reaction, this might eventually result in high 2-cyclohexen-1-ol selectivity and low cyclohexene oxide selectivity. On the contrary, at the H_2O_2-to-cyclohexene ratio lower than optimum value of 1, the surface oxygen transfer reaction to form cyclohexene oxide as the main product might predominantly occur, while the difference due to auto-oxidation might be reasonably negligible because most of H_2O_2 used probably underwent *tert*-butyl peroxotitanium complex formation for surface cyclohexene epoxidation. Consequently, the high cyclohexene oxide selectivity was attained with low undesired product selectivities, while the total amount of convertible cyclohexene through the combination of surface epoxidation and auto-oxidation at H_2O_2-to-cyclohexene ratio less than value of 1 might be insignificantly different. Therefore, it can be concluded that at the optimum reaction conditions (reaction temperature,

70°C; catalyst, 0.50 g; and H_2O_2-to-cyclohexene ratio, 1) under the investigated system, the RuO_2/TiO_2 (IWI) was verified to be a promising catalyst with high catalytic performance for cyclohexene epoxidation with H_2O_2.

4.3.7 Recycling of the Spent Catalysts

The recyclability test of 1 mol% RuO_2/TiO_2 (IWI) and RuO_2/TiO_2 (SSSG) calcined at 550°C for 4 h for cyclohexene epoxidation with H_2O_2 in *tert*-butanol was also tested for three cycles at the obtained optimum reaction condition. The catalysts recovered from the reaction mixture by centrifuging, and the recovered catalysts were washed with *tert*-butanol and then with distilled water to remove all of the organic phases adsorbed on the catalyst and dried at room temperature. The cyclohexene conversion and product selectivity of 1 mol% RuO_2/TiO_2 (IWI) and 1 mol% RuO_2/TiO_2 (SSSG) are given in Figures 4.27 and 4.28, respectively. It was found that RuO_2/TiO_2 (IWI) exhibits slight decrease in cyclohexene conversion with significant decrease in cyclohexene oxide selectivity to 47.36 and 27.43% in the second and third cycles, respectively. On the other hand, RuO_2/TiO_2 (SSSG) exhibits almost unchanged in both conversion and selectivity, indicating its higher stability. This can be attributed by XRF analysis, shown in Table 4.8, namely, the significant loss of RuO_2 from the surface of catalyst in RuO_2/TiO_2 (IWI) affected to selectivity, but RuO_2/TiO_2 (SSSG) showed the only small loss of RuO_2 in the recycle process. Since 1 mol% RuO_2/TiO_2 (SSSG) showed high performance about recyclability test, much effort has been devoted to the development of this catalyst for cyclohexene epoxidation in order to obtain high cyclohexene conversion and cyclohexene oxide selectivity.

Table 4.8 Summary of RuO_2 weight loss (%) of RuO_2/TiO_2 (IWI) and RuO_2/TiO_2 (SSSG)

Catalyst	Cycle	Weight loss of RuO_2 (%)
RuO_2/TiO_2 (IWI)	1st	16.86
	2nd	36.78
RuO_2/TiO_2 (SSSG)	1st	0.99
	2nd	1.71

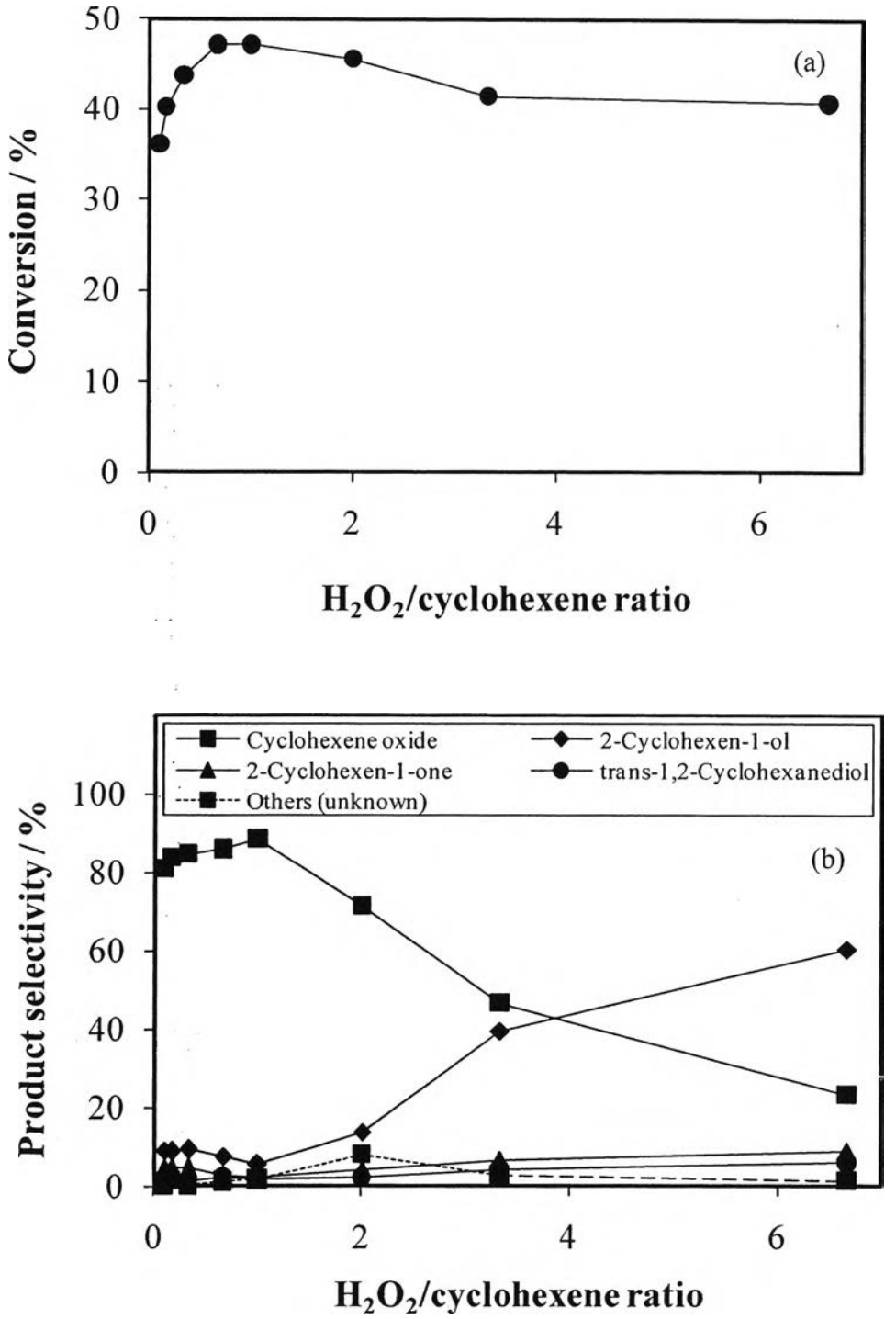

Figure 4.26 Effect of H_2O_2-to-cyclohexene ratio on cyclohexene epoxidation catalyzed by 1 mol% RuO_2/TiO_2 (IWI) calcined at 550°C for 4 h: (a) cyclohexene conversion and (b) product selectivity. Reaction conditions: cyclohexene 30 mmol; *tert*-butanol 30 ml; catalyst 0.5 g; reaction temperature 70°C; reaction time 5 h.

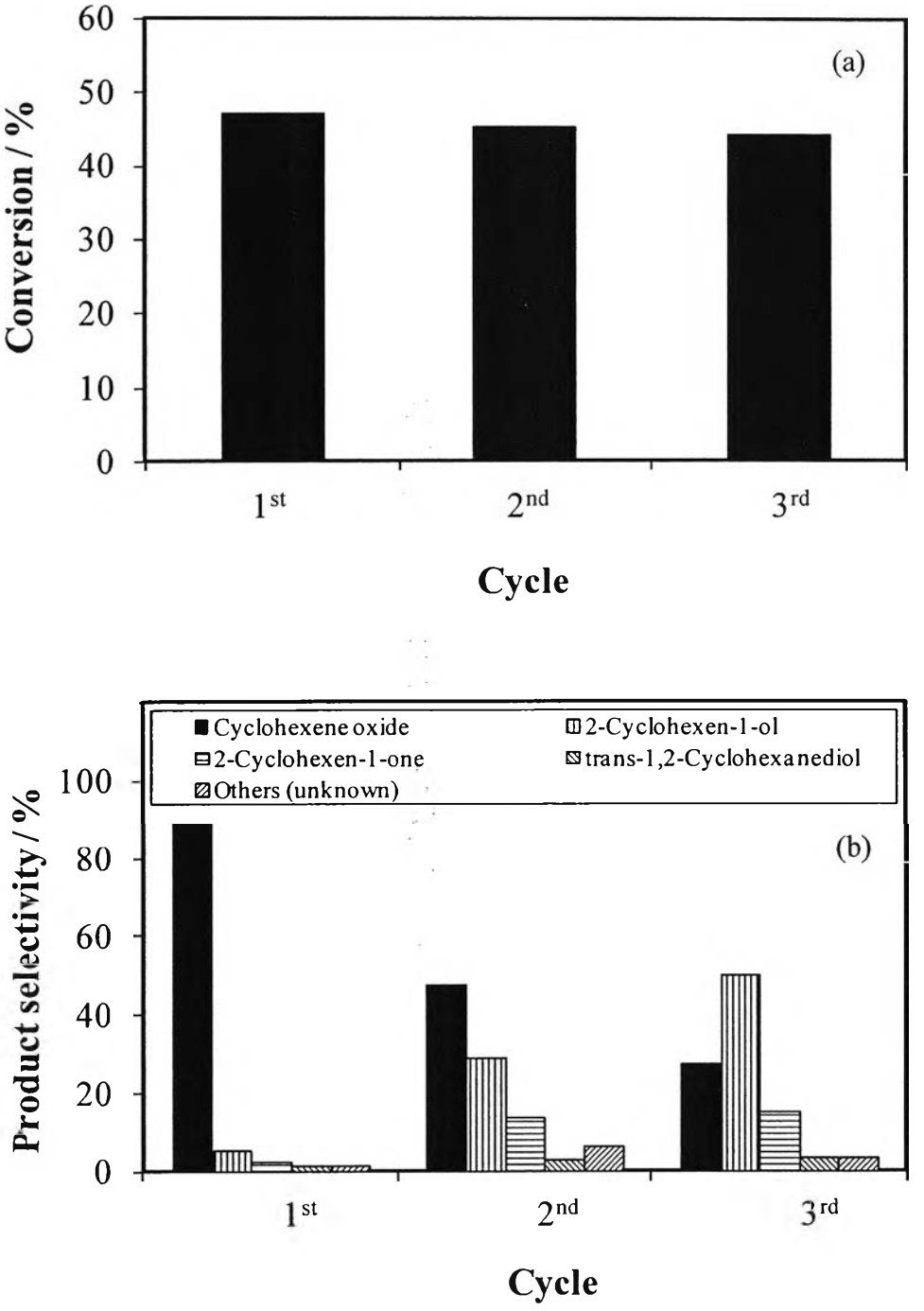

Figure 4.27 Recyclability of 1 mol% RuO_2/TiO_2 (IWI) calcined at 550°C for 4 h: (a) cyclohexene conversion and (b) product selectivity. Reaction conditions: cyclohexene 30 mmol; *tert*-butanol 30 ml; catalyst 0.5 g; reaction temperature 70°C; reaction time 5 h.

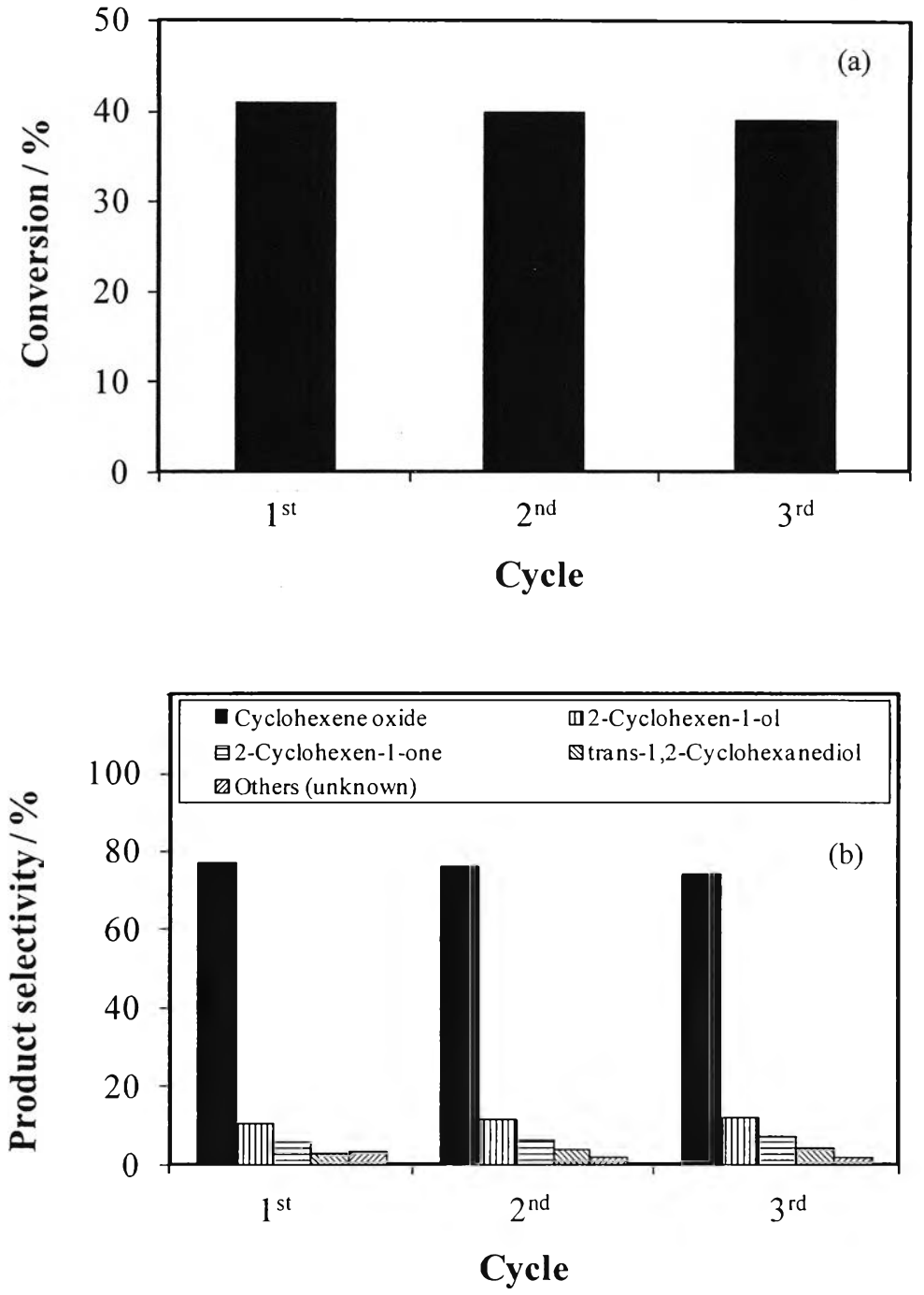

Figure 4.28 Recyclability of 1 mol% RuO_2/TiO_2 (SSSG) calcined at 550°C for 4 h: (a) cyclohexene conversion and (b) product selectivity. Reaction conditions: cyclohexene 30 mmol; *tert*-butanol 30 ml; catalyst 0.5 g; reaction temperature 70°C; reaction time 5 h.

4.4 Characterization and Catalytic Activity Results of RuO_2/TiO_2 (SSSG)

Among all the investigated catalytic activity of cyclohexene epoxidation concluded that 1 mol% RuO_2/TiO_2 (IWI) calcined at 550°C for 4 h showed the highest cyclohexene oxide selectivity. However, from the experimental results of recyclability test of the catalyst for cyclohexene epoxidation with H_2O_2 in *tert*-butanol, it can be found that 1 mol% RuO_2/TiO_2 (SSSG) calcined at 550°C for 4 h is stable and can be re-used in at least three reactions when compared with RuO_2/TiO_2 (IWI). Therefore, RuO_2/TiO_2 (SSSG) was taken to study the effect of calcination temperature in order to improve the catalytic activity of cyclohexene epoxidation. The different calcination temperatures of RuO_2/TiO_2 (SSSG) ranging from 400 to 550°C were investigated.

The thermogravimetry and differential thermal analysis (TG-DTA) was employed for determination of the surface OH density (OH/nm^2) and surface OH-to-catalyst weight ratio (OH/g). Figure 4.29 shows TGA curves of 1 mol% RuO_2/TiO_2 (SSSG). Moreover, the details of the surface OH density (OH/nm^2) and surface OH-to-catalyst weight ratio (OH/g) are summarized in Table 4.9.

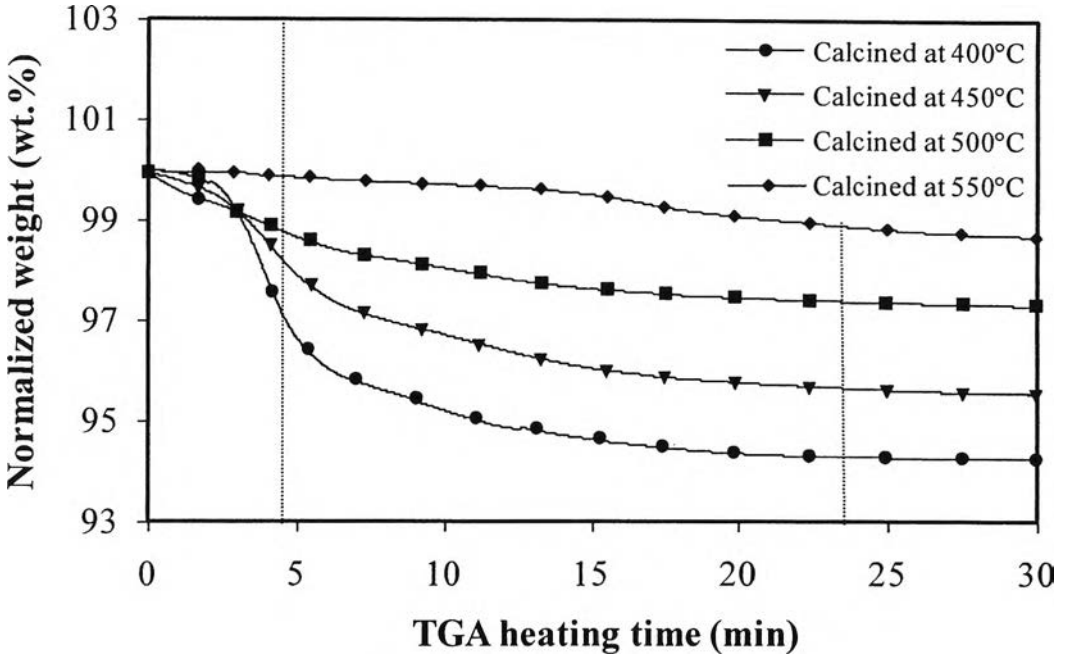

Figure 4.29 TGA comparison of 1 mol% RuO_2/TiO_2 (SSSG) calcined for 4 h with different calcination temperatures. The surface OH is based on the weight loss of between 120 and 500°C.

Table 4.9 Surface OH density (OH/nm^2) and surface OH-to-catalyst weight ratio (OH/g) of 1 mol% RuO_2/TiO_2 (SSSG) calcined for 4 h with different calcination temperatures

Catalyst	RuO_2 content (mol%)	Calcination temperature (°C)	Calcination time (h)	$w_{120°C}$ (mg)	$w_{500°C}$ (mg)	OH/nm^2	$OH/g(\times10^{-20})$
RuO_2/TiO_2 (SSSG)	1	400	4	14.00	13.74	6.77	8.54
		450		11.64	11.45	7.55	7.42
		500		11.39	11.27	7.94	4.78
		550		21.94	21.70	18.19	4.73

The results from TGA analysis show the change of surface OH-to-catalyst weight ratio (OH/g) with respect to the calcination temperatures. It can be

clearly seen that surface OH-to-catalyst weight ratio (OH/g) decreased with increasing the calcination temperature.

The N_2 adsorption-desorption isotherms of the 1 mol% RuO_2/TiO_2 (SSSG) calcined at 450°C for 4 h, providing the best catalytic activity performance for cyclohexene epoxidation as next discussed, also exhibited typical IUPAC type IV pattern with hysteresis loop, which is characteristic of mesoporous-assembled structure (mesoporous size between 2-50 nm) according to the classification of IUPAC (Rouquerol *et al.*, 1999), as shown in Figure 4.30. The inset of Figure 4.30 shows pore size distribution curve calculated from the desorption branch of isotherms by the BJH method. The samples possess monomodal and very narrow pore size distribution, identifying good quality of the sample.

The experimental results on textural properties of all investigated 1 mol% RuO_2/TiO_2 (SSSG), including BET surface area, mean pore diameter, and total pore volume, are shown in Table 4.10.

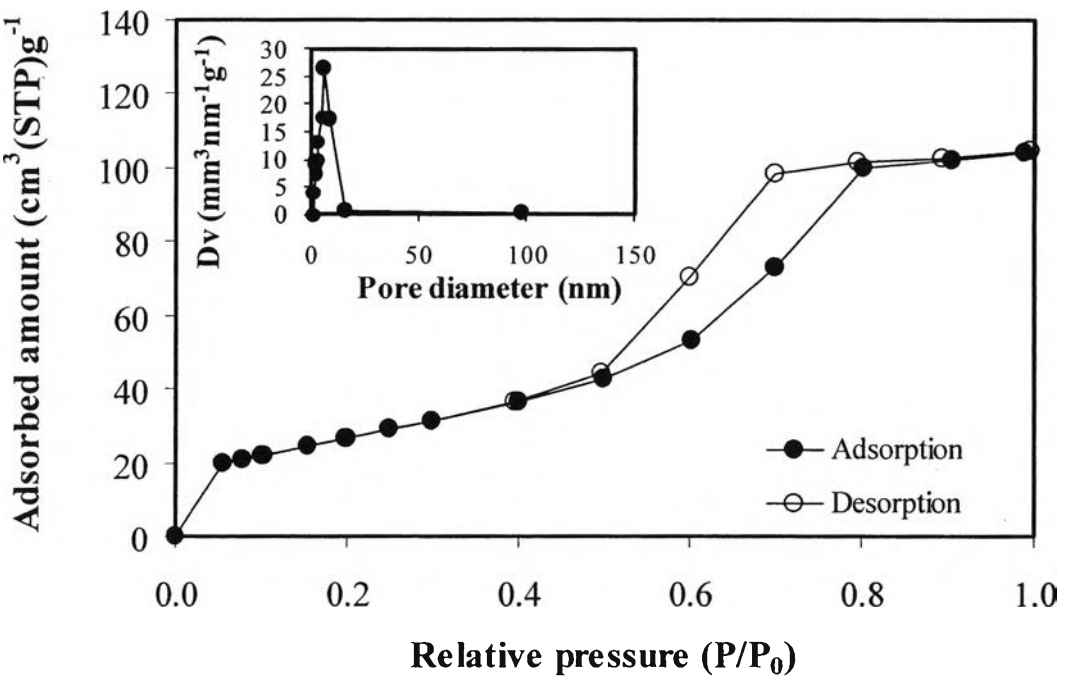

Figure 4.30 N_2 adsorption-desorption isotherms of the 1 mol% RuO_2/TiO_2 (SSSG) calcined at 450°C for 4 h (Inset: pore size distribution).

Table 4.10 Summary of textural properties obtained from N_2 adsorption-desorption results of 1 mol% RuO_2/TiO_2 (SSSG) calcined for 4 h with different calcination temperatures

Catalysts	RuO_2 content (mol%)	Calcination temperature (°C)	Calcination time (°C)	BET surface area ($m^2 \cdot g^{-1}$)	Mean pore diameter (nm)	Total pore volume ($cm^3 \cdot g^{-1}$)
RuO_2/TiO_2 (SSSG)	1	400	4	126.20	6.25	0.20
		450		98.41	6.54	0.16
		500		60.13	8.24	0.12
		550		26.02	10.52	0.06

The results from N_2 adsorption-desorption analysis showed the change of surface area with respect to the different calcination temperatures. As obviously seen, the surface area of the 1 mol% RuO_2/TiO_2 (SSSG) decreased from 126.20 to 26.02 $m^2 \cdot g^{-1}$ with increasing calcination temperature from 400 to 550°C. With increasing the calcination temperature, the perceived loss in surface area is explainable to the pore coalescence due to the crystallization of walls separating mesopores. Moreover, the sintering and phase transformation of anatase to rutile phase are concerned (Lin *et al.*, 2007). Subsequently, this tendency caused an increase in mean pore diameter and a decrease in total pore volume of the bulk materials, as expected.

The XRD patterns of 1 mol% RuO_2/TiO_2 (SSSG) calcined for 4 h with different calcination temperatures are shown in Figure 4.31. Table 4.11 also summarizes all results of XRD analysis, including phase from XRD patterns, rutile ratio, and crystallite size.

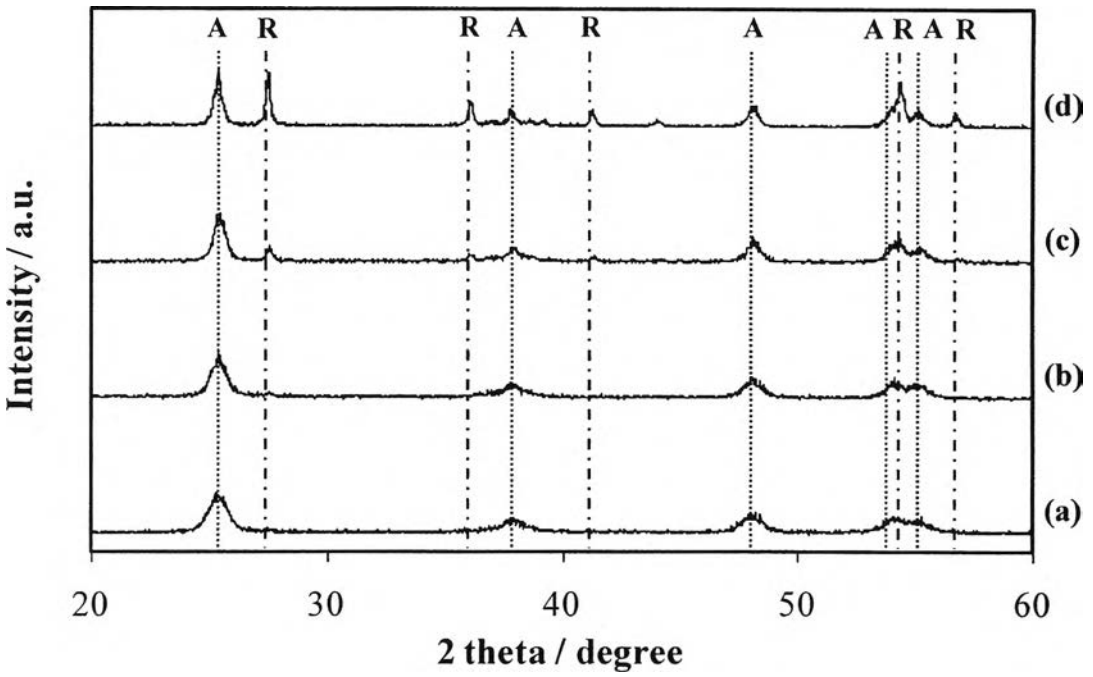

Figure 4.31 XRD patterns of 1 mol% RuO_2/TiO_2 (SSSG) calcined for 4 h with different calcination temperatures: (a) 400°C, (b) 450°C, (c) 500°C, and (d) 550°C (A: Anatase, R: Rutile).

The results from XRD patterns of 1 mol% RuO_2/TiO_2 (SSSG) calcined for 4 h with different calcination temperatures showed that the dominant peak of RuO_2 at 2θ of about 28.1 and 35.1° which represent the indices of (110) and (101) planes respectively, could not be observed due to the combination of its low content, high dispersion degree, and small particle size. The main peaks of 1 mol% RuO_2/TiO_2 (SSSG) at 2θ of 25.4, 37.9, 48.1, 53.9, and 55.3°, which represent the indices of (101), (004), (200), (105), and (211) planes respectively, are ascribed to structure of anatase TiO_2. However, it is evident that the calcination temperature of 500°C is the starting point of phase transformation from anatase to rutile phase since approximately 26% rutile content was observed. At the calcination temperature 550°C, partial phase transformation from anatase to rutile was observed, resulting in combination between anatase and rutile phases with approximately 61% rutile content which indicates that rutile phase becomes the main phase calcined at this temperature. Therefore, it can be explained that RuO_2/TiO_2 (SSSG) accelerated the

rutile phase. Moreover, the results also reveal that with increasing calcination temperature, the larger TiO_2 crystallite size was obtained.

Table 4.11 Summary of XRD analysis of the 1 mol% RuO_2/TiO_2 (SSSG) calcined for 4 h with different calcination temperatures (A: Anatase, R: Rutile)

Catalysts	RuO_2 content (mol%)	Calcination temperature (°C)	Calcination time (°C)	Phase from XRD Pattern	Rutile ratio (W_R)	Crystallite size (nm)	
						Anatase (101)	Rutile (110)
RuO_2/TiO_2 (SSSG)	1	400	4	A	-	8.647	-
		450		A	-	10.59	-
		500		A+R	0.26	14.07	26.72
		550		A+R	0.61	20.61	33.17

The catalytic activity of cyclohexene epoxidation when 1 mol% RuO_2/TiO_2 (SSSG) calcined for 4 h with different calcination temperatures are shown in Figure 4.32. It can be concluded that 1 mol% RuO_2/TiO_2 (SSSG) calcined at 450°C for 4 h provided the highest both cyclohexene conversion and cyclohexene oxide selectivity when compared with the other calcination temperatures. At the calcination temperature of 400°C, the crystallization to anatase phase of the synthesized catalyst may not be fully developed and this temperature was not sufficient for complete surfactant template removal shown in Figure 4.2. Moreover, at the calcination temperature of 500 and 550°C, transformation from anatase phase to rutile phase was observed, resulting in combination between anatase and rutile phases shown in Figure 4.31, namely, the presence of rutile phase can disadvantageously influence on the low catalytic performance because the less degree of hydroxyl group of the rutile structure rather than the anatase one.

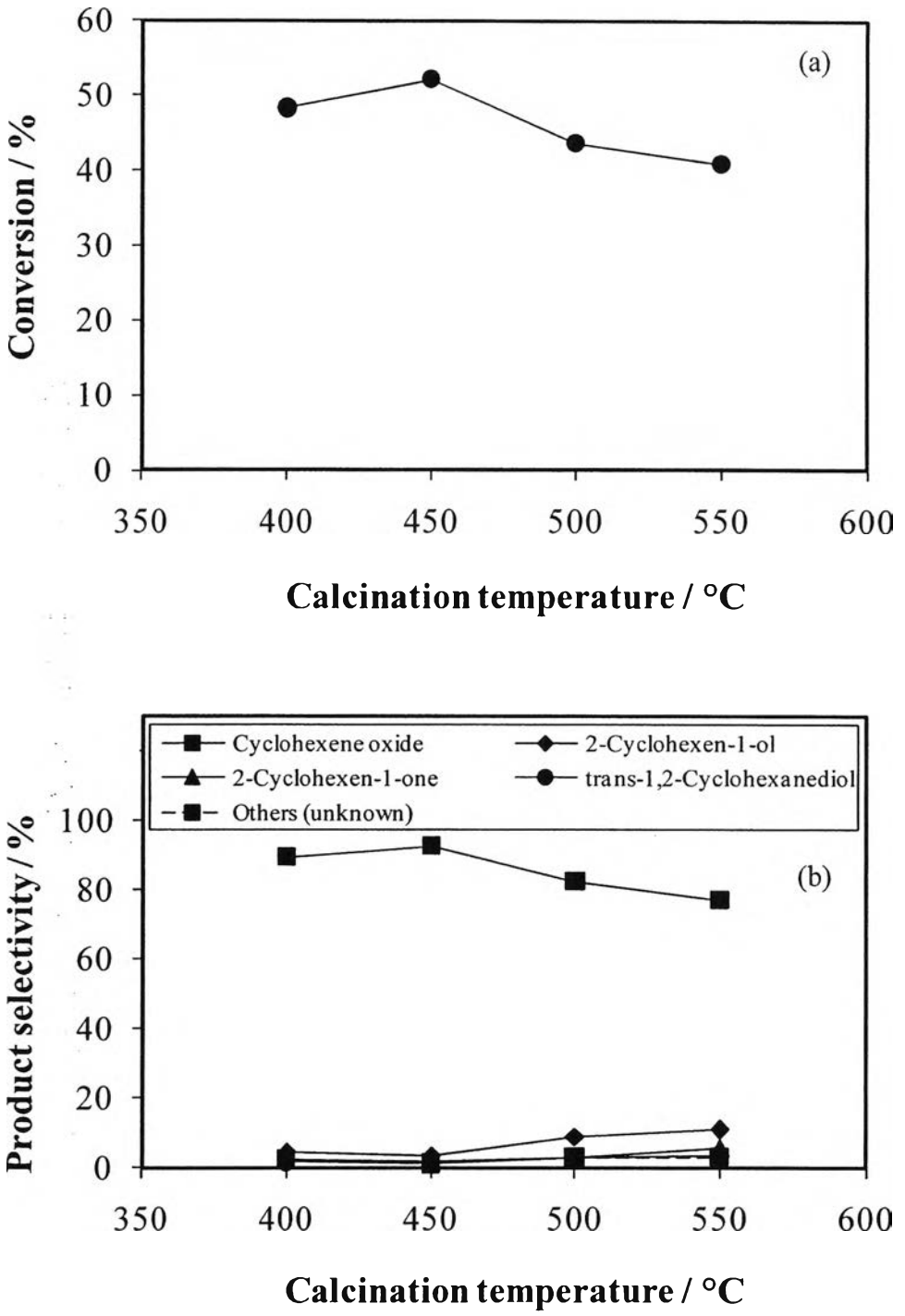

Figure 4.32 Cyclohexene epoxidation catalyzed by 1 mol% RuO_2/TiO_2 (SSSG) calcined for 4 h with different calcination temperatures: (a) cyclohexene conversion and (b) product selectivity. Reaction conditions: cyclohexene 30 mmol; *tert*-butanol 30 ml; H_2O_2 30 mmol; catalyst 0.5 g; reaction temperature 70°C; reaction time 5 h.